NUREG/CR-2857
BNL-NUREG-51571

LWR STEAM SPIKE PHENOMENOLOGY: DEBRIS BED QUENCHING EXPERIMENTS

T. Ginsberg, J. Klein, J. Klages,
C.E. Schwarz, and J.C. Chen

Date Published — June 1982

DEPARTMENT OF NUCLEAR ENERGY, BROOKHAVEN NATIONAL LABORATORY
UPTON, NEW YORK 11973

Prepared for
U.S. Nuclear Regulatory Commission
Washington, D.C. 20555

NUREG/CR-2857
BNL-NUREG-51571
AN,R2

LWR STEAM SPIKE PHENOMENOLOGY: DEBRIS BED QUENCHING EXPERIMENTS

T. Ginsberg, J. Klein, J. Klages, C.E. Schwarz, and J.C. Chen

Manuscript Completed — May 1982
Date Published — June 1982

EXPERIMENTAL MODELING GROUP
DEPARTMENT OF NUCLEAR ENERGY
BROOKHAVEN NATIONAL LABORATORY
UPTON, NEW YORK 11973

Prepared for
OFFICE OF NUCLEAR REGULATORY RESEARCH
U.S. NUCLEAR REGULATORY COMMISSION
WASHINGTON, D.C. 20555
UNDER INTERAGENCY AGREEMENT DE-AC02-76CH00016
NRC FIN NO. A-3024

DISCLAIMER

Printed in the United States of America
Available from
National Technical Information Service
U.S. Department of Commerce
5285 Port Royal Road
Springfield, VA 22161

NTIS price codes:
Printed Copy: A05; Microfiche Copy: A01

ABSTRACT

An experimental investigation is reported whose objective is to provide an understanding of the thermal interaction between superheated core debris and water during postulated light-water reactor degraded core accidents. The experiment was designed to study the heat transfer characteristics of superheated spheres as they are quenched in a packed bed configuration by an overlying pool of water. The results of the experiment are applied to understanding of the containment "steam spike" phenomenon.

Three-millimeter stainless steel spheres were heated in an oven to temperatures between 533 K and 977 K, and subsequently transferred to a vertical 108.2 mm i.d. stainless steel vessel. Water at temperatures between 274 K and 360 K was released on to the spheres and the resulting thermal interaction was observed. Packed beds were studied whose nominal heights were in the range 200 mm to 400 mm. The experiments were carried out at constant pressure, with the steam vented to the atmosphere. The wall of the test vessel could be preheated, if desired, to match the initial sphere temperature. The test section was instrumented with an array of thermocouples, both within the vessel and on its outside wall. A pressure transducer was mounted on the test vessel wall to monitor pressure fluctuations indicative of continued boiling within the vessel.

Bed and wall temperature traces are presented for a range of experimental conditions. The bed thermocouples show a sequence of step changes in temperature, beginning with the uppermost one in the bed and proceeding downward. The temperatures suddenly drop from their initial values to the liquid saturation temperature. This sequential pattern of temperature reductions is interpreted to be indicative of a frontal cooling pattern which propagates down the column. The position of the front as a function of time is obtained from analysis of the temperature traces and are presented as frontal propagation plots for each experimental run.

The temperature traces and frontal propagation plots indicate that the downward-moving front arrives at the base of the bed after a time delay which depends on the bed depth and initial particle temperature. In many of the experiments the thermocouples indicate that a second front then moves up the column. The position of this front vs. time is extracted from the thermocouple data. The particle quench process is complete after passage of the upward-propagating front.

The heat transfer rate from the particle bed to water is estimated to have been in the range 1.0×10^6 to 2.5×10^6 W/m^2, independent of the initial particle temperature. The higher figure is an upper bound estimate of the heat transfer rate. The lower number of 10^6 W/m^2 represents an estimate of the average heat transfer rate over the duration of an experiment. This quantity is in reasonable agreement with predictions based upon steady-state debris bed heat transfer models and experimental data, suggesting that two-phase countercurrent flow is also a limiting factor in the transient heat removal from debris beds.

The data suggest that the cooling rate of superheated particle beds, and hence the rate of steam generation, is limited by supply of liquid to the dry region of the bed. It is plausible that the supply of liquid, in the transient cooling experiments, is limited by a countercurrent two-phase flow mechanism. Additional data are required for further substantiation of this hypothesis.

These transient particle bed quenching experiments suggest that the LWR containment steam spike pressurization rate would be limited by supply of liquid to the dry region of the debris bed. The bed behavior observed in this work, however, implies that solid particle debris would thermally attack the concrete basemat upon contact. The gases released from the concrete may further limit or preclude further bed cooling.

TABLE OF CONTENTS

TABLE OF CONTENTS
(Cont'd)

LIST OF FIGURES

LIST OF FIGURES
(Cont'd)

LIST OF TABLES

NOMENCLATURE

A	Particle bed cross-sectional area
A_p	Single particle surface area
c	Particle specific heat
d	Particle diameter
f_d	Fraction of stored energy transferred during downward-frontal period
h_{fb}	Film boiling heat transfer coefficient
H	Bed height
m_p	Single particle mass
M	Total mass of bed particles
q''_d	Heat flux during downward-propagation period
Q	Bed stored energy content
t	Time
t_d	Time for downward-directed front to traverse bed
t_{fall}	Particle fall time
t_q	Particle bed quench time
t_q^{TC}	Particle bed quench time as determined from thermocouples
t_u	Time for upward-directed front to traverse bed
T	Temperature
T_o	Initial particle temperature
T_{SAT}	Water saturation temperature
T_{ZERO}	$\equiv T_o$
v_d	Speed of downward-directed front
v_u	Speed of upward-directed front

NOMENCLATURE
(Cont'd)

Greek Symbols

ϵ	Particle bed porosity
ρ	Particle density
τ_p	Single particle heat transfer time scale

1. INTRODUCTION

1.1 Motivation for Research

Analyses of core meltdown accidents in light water reactors (LWRs) are being performed to develop an understanding of the consequences of such postulated accidents. Studies of meltdown accidents are being sponsored by the Nuclear Regulatory Commission in conjunction with their program on Severe Accident Mitigation Features for the Zion and Indian Point pressurized water reactor (PWR) power plants (Denton, 1980; Meyer, 1981). Analysis of containment building pressurization as a result of loadings imposed by the core melt is an integral feature of these studies. A source of containment pressurization of major concern is that of steam generation as a result of quenching (removal of stored energy) of the hot core debris with available cooling water. The phenomenology of the quench process, sometimes referred to as the "steam spike", is incompletely understood. The objective of the work described here is to develop and evaluate mechanistic models which characterize the thermal interaction between core debris and water. These models will be incorporated into containment analysis computer codes.

1.2 Background

1.2.1 A LWR Meltdown Accident Sequence

A number of LWR accident sequences have been identified which lead to complete core meltdown (Rasmussen, 1975). Among these, the "TMLB'" accident progression has been most widely studied. TMLB' is considered here because of the potential importance of the steam spike phenomenon to the consequences of the accident, and because of its importance to the Zion - Indian Point Study. The accident sequence outlined below is discussed in detail by Meyer (1981) and Pratt (1981).

The TMLB' accident progression is initiated by loss of offsite electrical power, followed by failure to recover either onsite or offsite power. This results in loss of secondary heat removal capability and leads to primary system pressurization under decay heating conditions. The pressurizer relief valves open at their pressure set point and blowdown of primary steam to the containment building occurs. Core uncovery ensues, followed by heatup and relocation of fuel and structural material within the reactor vessel. Molten fuel and structural material eventually slump into the lower plenum and thermally interact with the available water. The water would be completely vaporized and the fuel and metal partially quenched. The steam produced would provide an additional loading on the containment building.

Figure 1.1 is an accident sequence flow chart for the time period subsequent to vaporization of remaining water from the reactor vessel. The hot debris would heat the reactor vessel, which would fail by one of the modes postulated in Fig. 1.1 and shown graphically in Fig. 1.2 (Corradini, 1980). The debris would drop out of the vessel into the reactor cavity. Following vessel failure, the remaining primary water would flash into the containment building. Primary system pressure would be reduced, the accumulators would release their water to the vessel and thereby to the reactor cavity. The core debris would

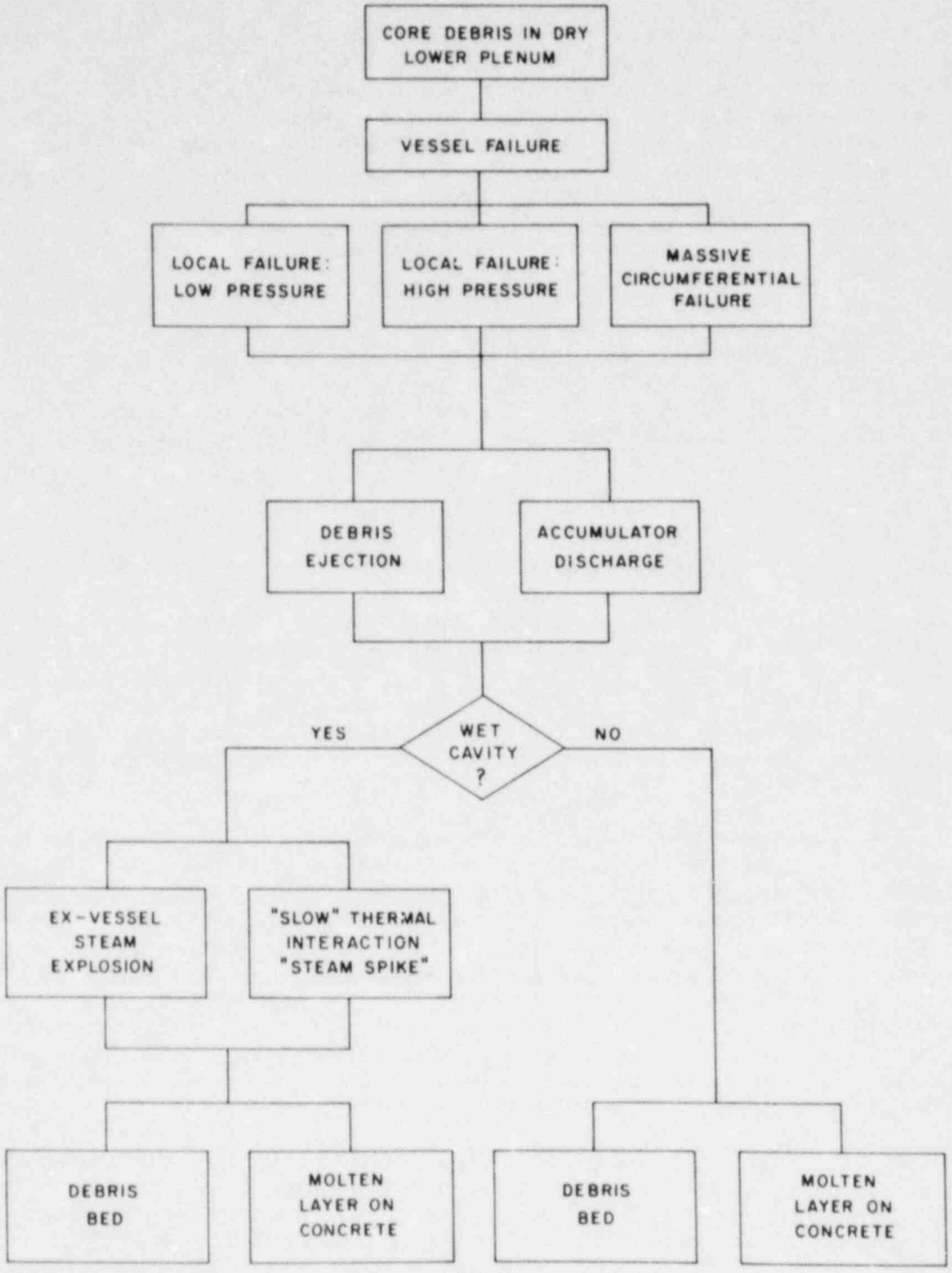

FIG. 1.1 Core Debris-Water Thermal Interaction Accident Sequence

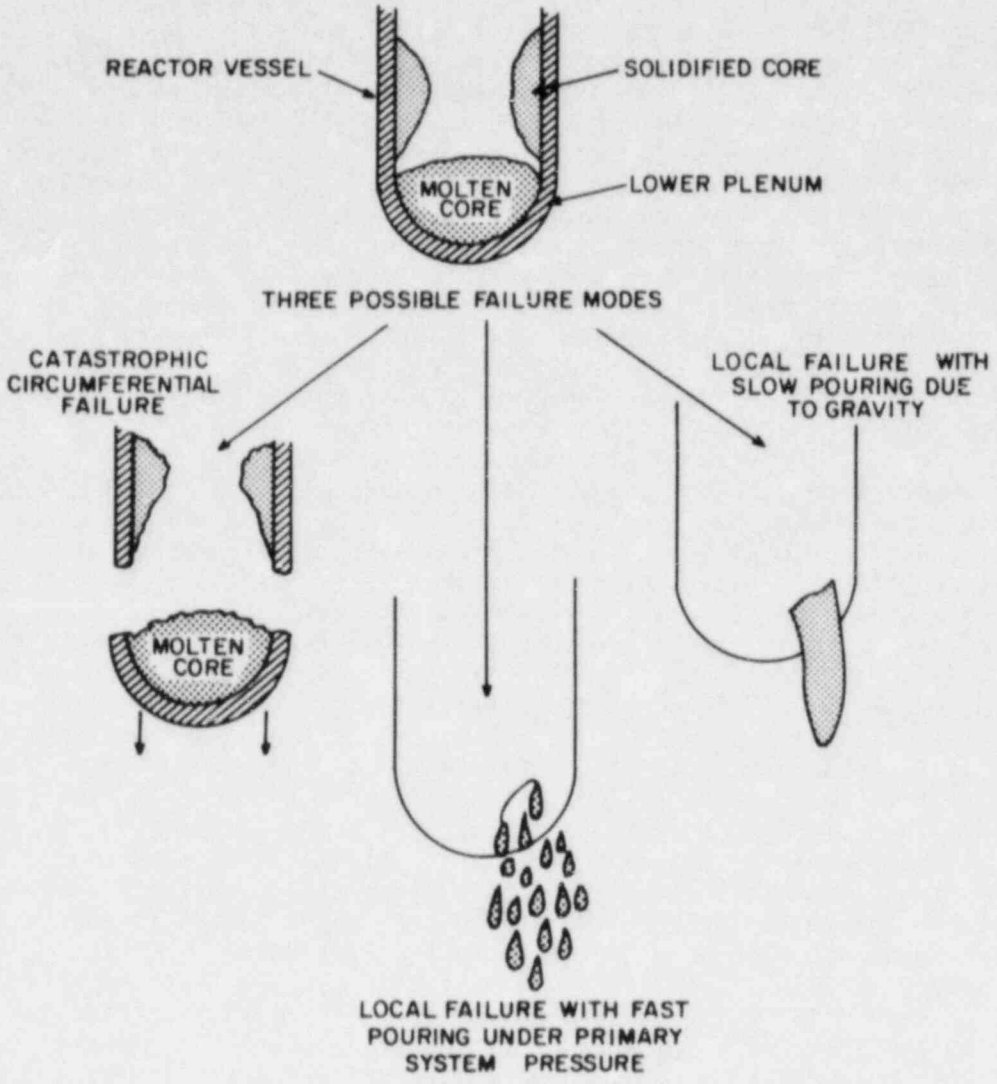

FIG. 1.2 Modes of Reactor Vessel Failure
(Corradini, 1980)

interact with water available in the cavity, producing steam and pressurizing the containment building. The debris would attack the concrete and decomposition gases would provide an additional pressure loading on the containment building if cooling water is not available to cool the cavity concrete basemat. Following quenching of the core debris, decay heating would continue to pressurize the containment building if cooling water is available.

Figure 1.1 shows two paths for the interaction between water and core melt in the reactor cavity: (i) a steam explosion, or (ii) "slow" non-explosive thermal interaction. It is known that steam explosions may accompany the thermal interaction between molten core material and water (Corradini, 1980). Uncertainties exist, however, in the prediction of the conditions required for a steam explosion, and of the rate processes involved in the interaction. Whether or not a steam explosion occurs under given conditions would significantly influence the subsequent thermal characteristics of the debris. The extent of debris fragmentation, for example, appears to depend on whether the interaction is explosive or not. Steam explosions lead to much smaller fragment sizes than debris characteristic of "slow" thermal interactions (Mitchell, 1981). The present work focuses on the description of non-explosive thermal interaction between core debris and water. Containment loading mechanisms due to steam explosions are beyond the scope of the present work.

The MARCH code (Wooton, 1980), which incorporates simplified models for the various phenomena, has been used to compute the containment pressure history resulting from postulated TMLB' accidents in the Zion and Indian Point plants (Yang, 1981). A typical calculation result is shown in Fig. 1.3. The segment a-b of the pressure history corresponds to the blowdown phase, during which primary steam is discharged through the pressure relief valve. At 'b' the core is uncovered and vaporization can no longer proceed. Condensation leads to the small drop in pressure in segment b-c. The molten core is assumed to drop into the lower plenum at 'c', leading to steam generation and a 0.09 MPa (13 psi) pressure rise in the containment building. The reactor vessel is assumed to fail two minutes following deposition of the core on the lower vessel head. The remaining primary system water flashes, leading to an additional 0.1 MPa (15 psi) loading on the containment building. The segment c-d includes pressure rises from the lower plenum interaction and the primary water depressurization. The containment building pressure at this point is approximately 0.48 MPa (69 psia). The core debris falls from the vessel into the reactor cavity. For the calculation of Fig. 1.3, it was assumed that the cavity would contain primary water which would be diverted to the cavity rather than routed to the containment sump. The thermal interaction between the debris and water leads to the pressure rise of 0.26 MPa (38.0 psia), represented by segment d-e of Fig. 1.3. At 'e' the debris is quenched to the water saturation temperature. Further pressurization beyond 'e' occurs as a result of decay heating.

The pressure rise of 0.26 MPa resulting from the quenching of core debris is accompanied by vaporization of 8.5×10^4 kg of water in 42 seconds. This vaporization rate was computed using the HOTDROP model of the MARCH code to represent the thermal interaction. This model assumes that the core debris is fragmented into a collection of suspended spheres. Each sphere transfers energy independently to the water at a rate which is limited by boiling heat

transfer and radiation externally, and by thermal conduction internally. The large surface area of the debris leads to the large vaporization rates.

It was recognized (Yang, 1981) that the debris would eventually reach a settled bed configuration on the reactor cavity floor and that the steam generation rate from a bed configuration could be much lower than from suspended spheres. A factor of 10^3 lower surface area for debris beds of millimeter-scale diameter was expected to lead to lower containment pressurization rates. Debris bed limiting heat transfer models (Lipinski, 1980; Dhir, 1977; Dhir, 1979) were incorporated into the MARCH code by Yang (1981) and by Corradini (1980) and containment pressurization calculations were performed.

Typical calculational results taken from Yang (1981) are shown in Fig. 1.4, in which the HOTDROP results are compared with the debris bed model results. It is observed that the pressurization rate predicted by the single-particle and debris bed models is strongly model-dependent and is also a strong function of assumed particle size. The results also indicate, however, that the magnitude of the pressure rise due to the thermal interaction in the reactor cavity is nearly independent of the model used to represent the interaction. These two observations are explained by the fact that the PWR containment building is fabricated of reinforced concrete, which effectively insulates the containment volume. The pressure rise attributable to the steam spike occurs on a time scale which is too small for heat losses to reduce the peak pressure attained during the transient.

The assumption of mode of thermal interaction between debris and water, i.e., MARCH single-particle vs. debris bed, is seen to significantly affect the time to reach peak pressure. In the case of the MARCH model the interaction is completed (particles are quenched to water saturation temperature) in 10's of seconds, whereas the debris bed models predict that peak pressures are attained in approximately 20 to 150 minutes, depending on the model. If PWR containment buildings are designed or modified to allow venting to reduce pressures during postulated accidents, then this difference in time scales could be of major importance in specifying vent design criteria. Similarly, the pressurization rate would strongly influence design parameters of active or passive containment cooling systems if they should be chosen to mitigate the consequences of meltdown accidents. It is important, therefore, to characterize the thermal interaction between core debris and water using models which have been verified against experimental data.

1.2.2 Accident Sequence Uncertainties

The two models discussed in Section 1.2 have been applied using the MARCH code in order to bound the containment pressurization problem. The details of the preceding phases of the accident and their impact on the thermal interaction process have been ignored in prior analyses. In actuality, however, the mechanism of thermal interaction between debris and water upon release from the reactor vessel is expected to be closely tied to several factors which define the initial conditions for the interaction. These factors, some of which are identified below, depend on the details of earlier phases of the meltdown accident:

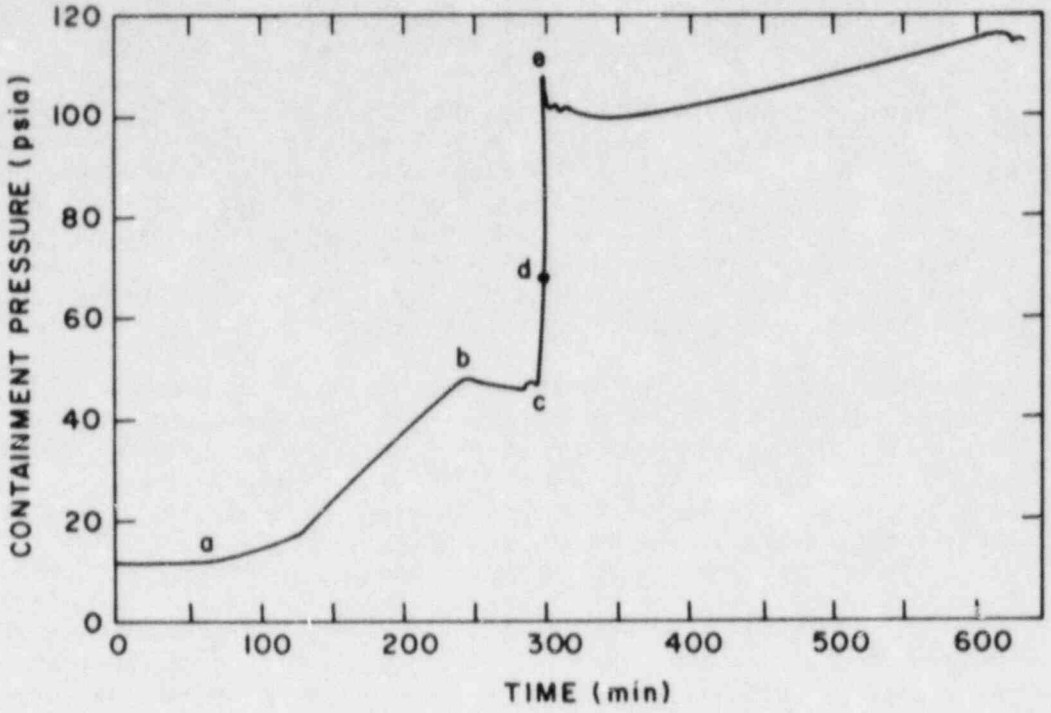

FIG. 1.3 MARCH Calculation of "Wet Cavity" Steam Spike Using HOTDROP Model (Yang, 1981)

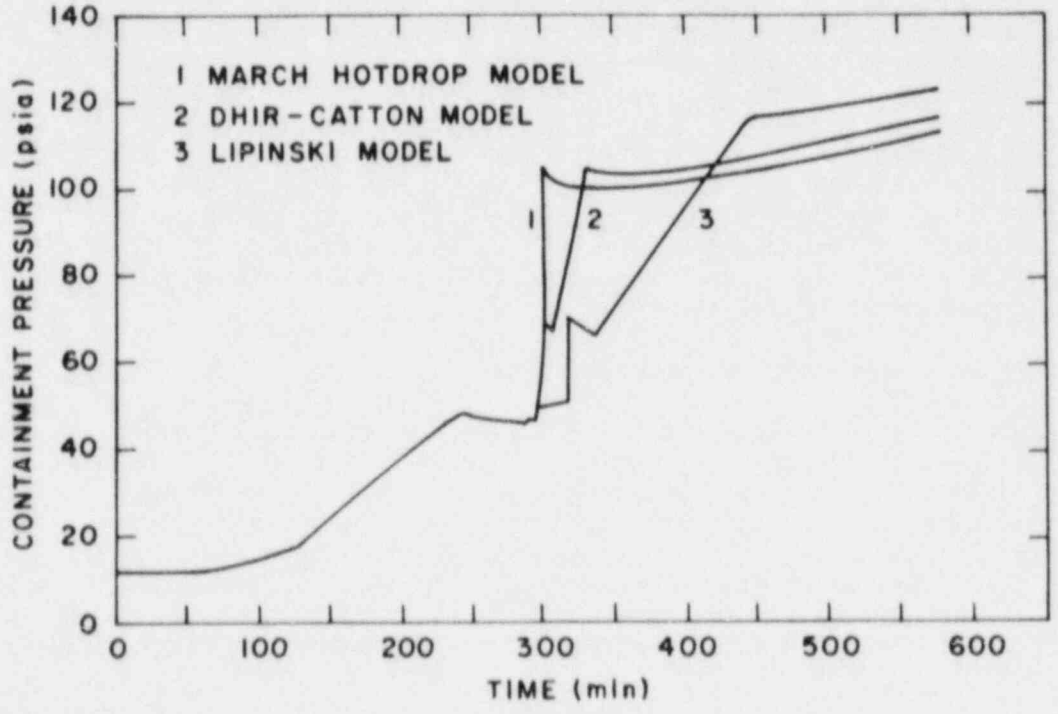

FIG. 1.4 Comparison of HOTDROP with Debris Bed Models for 5 mm Spheres (Yang, 1981)

(i) temperature and melt-solid composition of the debris prior to failure of the vessel;

(ii) mode of failure of the reactor vessel, e.g., local vs. massive failure;

(iii) extent of fragmentation of molten debris upon contact with water;

(iv) mode of contact of molten debris with water, e.g., jet penetration vs. well-mixed contact;

(v) inventory of water in the reactor cavity.

The factors listed above represent uncertainties which render detailed modeling of the thermal interaction process difficult. Sets of assumptions need to be made and several alternative accident sequences analyzed, in order to bound the consequences of the postulated accident.

Three basic debris-water thermal interaction sequences can be envisioned:

(i) Core debris drops into a dry reactor cavity, followed by introduction of water:

The melt would spread along the concrete floor of the cavity and would begin to interact with the concrete, as represented in Fig. 1.5(a). The subsequent behavior of the molten pool with gas evolution from concrete and with water available above the melt is not understood. Whether or not the molten pool configuration would cool as a pool or would mix with water, fragment and subsequently cool as particulate debris, as shown in Fig. 1.5(b), is not known.

(ii) Molten core falls into a water-filled cavity as a jet (diameter << lateral cavity dimensions):

This sequence could result from local vessel failure. If molten material penetrates the water as a jet with little breakup and mixing, then the melt could spread along the cavity floor, leading to a sequence similar to (i) above.

(iii) Molten core debris falls into an initially water-filled cavity and is followed by extensive mixing with water on a lateral scale on the order of that of the reactor vessel or reactor cavity.

This sequence postulates extensive intermixing between water and melt with fragmentation of the debris during the fall to the reactor cavity floor. This mode of contact would result in greater steam generation rates than (i) and (ii) above.

Of the three sequences characterized above, it is hypothesized that the third would lead to the largest rate of containment pressurization due to steam

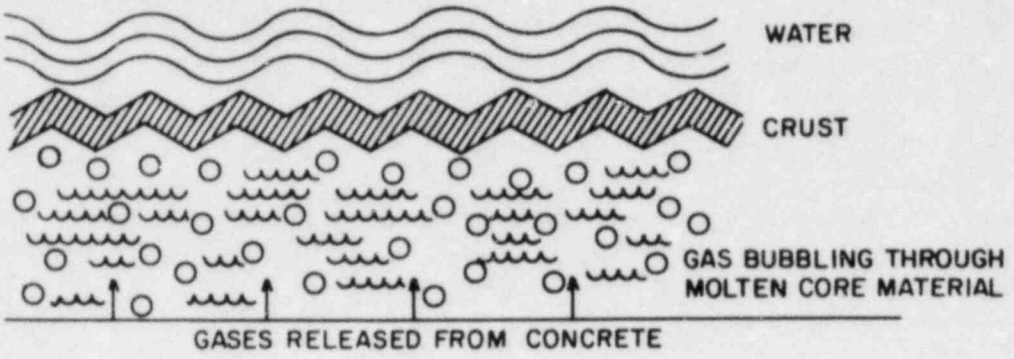

(a)

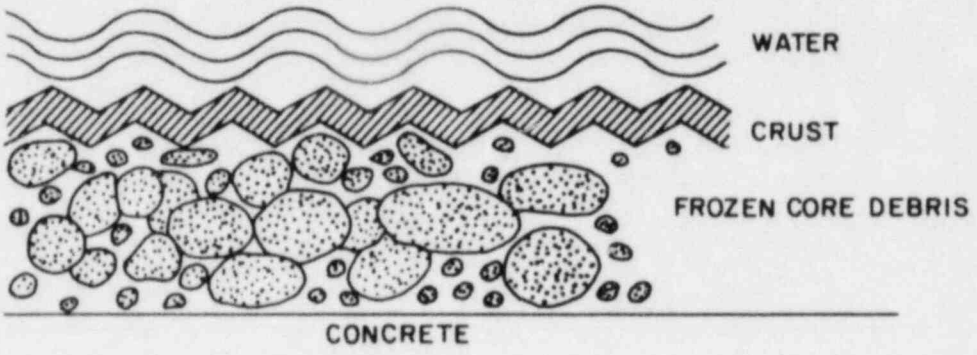

(b)

FIG. 1.5 Schematic Representation of Core Debris Resting on Concrete Basemat: (a) Molten Pool on Concrete; (b) Particulate Debris on Concrete (Meyer, 1981)

eration. The work reported here is directed to development of models which aracterize the thermal interaction postulated by this sequence. A model for nis thermal interaction is discussed in Section 2.1.

1.2.3 Thermal Interaction Model Uncertainties

In addition to the accident sequence uncertainties discussed above, uncertainties exist inherent in the use of two limiting models which have been used to characterize the interaction between debris and water.

The MARCH HOTDROP model assumes that each of the fragments of core debris is suspended in an infinite sea of water and that the heat transfer is limited by debris internal and external resistances. Steam production is assumed to be governed by the total surface area of the fragments. The fragments, however, are likely to be suspended in the fluid only for a limited time and would settle under gravity. The liquid pool is likely to be disrupted by large steam velocities produced by the thermal interaction. Debris-liquid contact is likely to be less than assumed in the HOTDROP model, and the steam generation rate could, therefore, be less than that predicted by HOTDROP.

The debris bed models which have been used to characterize the steam production rate of packed beds of particles were developed based upon steady state considerations and were evaluated against steady state experiments with internally heated particles. The validity of these models when applied to the transient cooling of debris beds has not been established by comparison with suitable transient experiments. In addition, it has been assumed that if the reactor cavity is flooded at all times, then water would wet the concrete, thereby preventing thermal attack and consequent gas release. It has not been established, however, that the debris bed behavior under transient quench conditions would permit water penetration to the bottom of the bed.

1.3 Outline of Remainder of Report

The objective of the remainder of this report is to describe a program of analysis and experimentation to develop models to predict the steam generation rate during quenching of core debris in water.

Chapter 2 presents the analysis which led to the conceptual design of the experimental program. The experimental apparatus and procedure are presented in Chapter 3. The results of the experiments are presented in Chapter 4 and discussed in Chapter 5. The implication of the results with respect to reactor safety are discussed in Chapter 6. Chapter 7 summarizes the results and highlights conclusions of the experimental study reported here.

2. ANALYSIS

2.1 Thermal Interaction Stages

Molten core debris which discharges from the reactor vessel is assumed to interact with the cooling water in the reactor cavity in four stages:

(i) initial fragmentation and mixing;

(ii) fall of fragments through pool of water;

(iii) debris bed sensible heat removal (quenching);

(iv) debris bed decay heat removal.

Stored energy is removed in the first three stages, while decay heat is removed in stage (iv). These stages are considered below.

2.2 Initial Fragmentation and Mixing

This stage is not considered in detail in this work. It is assumed, however, that the initial mixing process leads to fragmentation of the debris into particulates which are subsequently free to fall through the available liquid pool to the floor of the reactor cavity, where they establish a debris bed configuration.

Figure 2.1 shows fragment size distributions resulting from interactions of molten thermite with water. Interactions which lead to steam explosions result in fragments which are typically hundreds of microns in diameter. On the other hand, interactions which are non-explosive are found to lead to particle sizes which are in the millimeter diameter range. Consistent with the objective of the present study, it is assumed that the fragment size is characteristic of non-explosive interactions, i.e., millimeters in dimension. The fragments are modeled as a collection of spheres of characteristic diameter 'd'.

2.3 Fragment Fall Period

It is assumed that the fragments fall through the pool of water as a collection of spheres and transfer energy to boiling water at a rate determined by the total particle surface area and the heat transfer resistances internal and external to the fragments. (This mode of heat transfer parallels that modeled by the HOTDROP model of the MARCH code.) Figure 2.2 shows the assumed geometry for the interaction. The falling fragments are spread across a cross-sectional area, A. They are assumed to interact with the water in a one-dimensional mode, that is, the fragments fall through the water beneath them. It is assumed that the water within the volume, V, cannot be displaced to other regions of the pool. This one-dimensional constraint is felt to be conservative, since it does not allow water to be diverted away from the thermal interaction region.

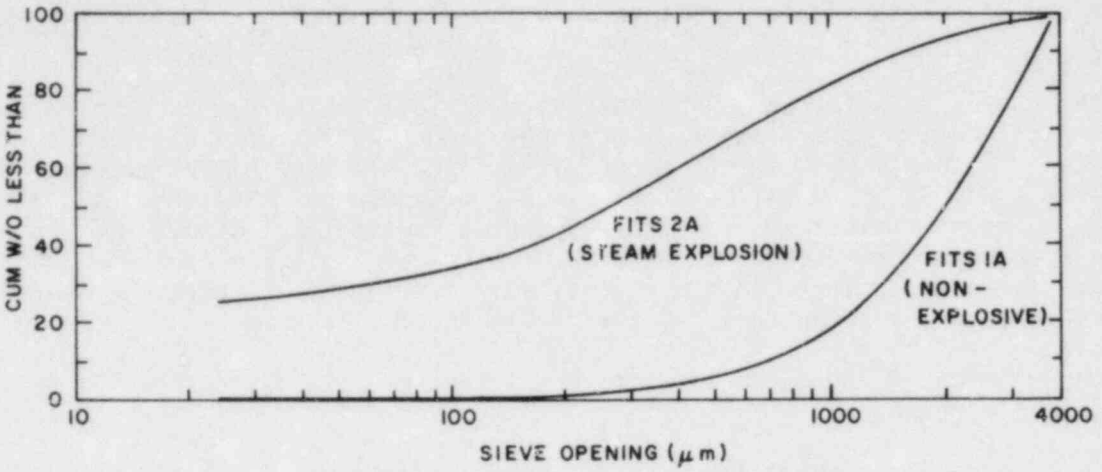

FIG. 2.1 Fragment Size Distribution from Iron-Alumina Thermite Experiments (Corradini, 1980)

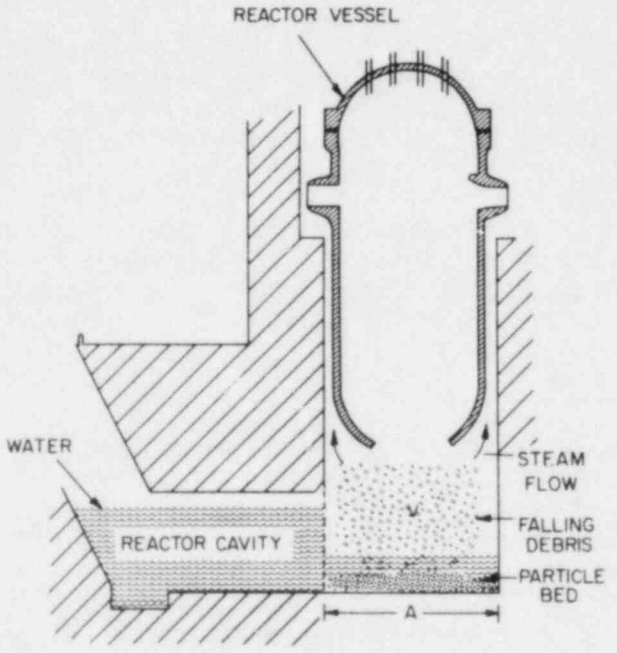

FIG. 2.2 Schematic Representation of Thermal Interaction Geometry Within Reactor Cavity

The fragmented debris lose a fraction of their initial stored energy during their fall to the floor of the reactor cavity. It is assumed that a "typical" fragment spends a time, t_{fall}, suspended in water prior to settling into a particle bed. The energy that can be removed from the particle during this period depends on the heat flux history of the fragments and on the fall time, t_{fall}.

The energy transferred during the fragment fall period can be significant. Calculations indicate, for example, that the time constant of a 3 mm UO_2 sphere in film boiling is on the order of seconds. If the initial temperature is 2477 K (4000 F), then half of the stored energy can be transferred to water in four seconds. This time scale corresponds approximately to the time required for the sphere to fall through 3-5 m of water available in the reactor cavity. It follows, then, that a significant fraction of the particle stored energy can be transferred to the water during the fall period.

Description of the particle-water heat transfer rate during the fragment fall period requires:

(i) a model for heat transfer between a collection of spheres falling through a pool of water, where the particles are initially in film boiling regime and where radiation is significant;

(ii) specification of the time scale that particles are suspended in the water prior to settling into a bed configuration.

Much information is available in the literature pertinent to boiling heat transfer from single spheres to infinite pools of water. There is no information, however, on the behavior of collections of spheres in bounded flow fields, where regions of the flow field are voided due to relatively large vapor fluxes.

The velocity of spheres falling through a two-phase liquid is probably not simply a function of the terminal velocity of the spheres in the pure liquid phase. A method for computation of the time period that particles are suspended in the two-phase flow prior to settlement must be developed.

2.4 Debris Bed Quench Period

The debris are assumed to settle into a packed bed configuration, having retained a fraction of their initial stored energy. The debris temperature is, for millimeter size fragments, likely to be above the minimum film boiling temperature upon establishment of the debris bed configuration. The debris are cooled by an overlying pool of water.

The steady state heat removal characteristics of internally heated debris beds have been widely studied. Models for the maximum heat removal rate from debris beds have been developed [see Gronager (1981) for summary]. There is general agreement that the heat removal rate is limited by two-phase countercurrent flow mechanisms. The specific dominant mechanisms, however, are not agreed upon, and the various models differ in their formulations. Table 2.1

TABLE 2.1

Dominant Forces in Debris Bed Heat Removal Models

Model	Forces Considered				Flow Regime	Comments
	Liquid-Particle	Vapor-Particle	Surface Tension	Liquid/Vapor		
Dhir-Catton (1979)	X				Laminar	
Lipinski (1980)	X	X	X		Laminar/Turbulent	
Hardee-Nilson (1977)	X	X			Laminar	
Gabor (1980)	X			X	Laminar	
Ostenson (1981)				X*	Turbulent	Based on flooding data from packed columns
Shires-Stevens	X	X	X		Laminar	
Theofanus (1981)		X*			Turbulent**	Based on flooding data from packed columns
Zuber (1959)				X***		Based on critical heat flux for flat plate

*Formulations for force models not given

**Not explicit, but apparently turbulent regime

***Hydrodynamic instability model used in analysis

lists the various models and dominant mechanisms considered. Figure 5.2 compares the maximum cooling rate of the various models.

The transient cooling behavior of superheated debris beds ($T_0 >> T_{SAT}$) has not been previously studied. Previous calculations (Yang, 1981), however, have assumed that the heat removal rate during bed quenching is limited by the same countercurrent flow mechanisms as discussed above for steady state conditions. The models listed in Table 2.1 were used to compute the steam generation rate during quench conditions. The prior calculations have also assumed that the concrete basemat on which the debris bed rests is adequately cooled, and that no gases are released. The implicit assumption is that water contacts the concrete during the quench process and provides the concrete cooling. The validity of these assumptions has not been evaluated.

A mathematical model for the transient quench behavior of superheated debris beds which are cooled by an overlying pool of coolant is required. The model should provide the steam generation rate for calculation of the containment building pressurization. It should, in addition, provide a basis for evaluation of the coolability of the concrete floor if liquid is available to the particle bed.

2.5 Debris Bed Decay Heat Removal

This stage of the interaction process is not of direct interest to this work. A brief discussion of relevant models is presented in Section 2.4 which refers to the relevant prior work in the area.

2.6 Combined Model

This work is directed to development of a model to characterize two phases of the thermal interaction between water and core debris -- the particle fall period and the debris bed quench period. The model will include:

(i) a description of heat transfer from a collection of superheated spheres falling through a two-phase pool of coolant, and the resulting steam generation rate;

(ii) a method for estimation of time-of-flight of spheres through the water prior to establishment of a debris bed;

(iii) a description of the heat removal characteristics of superheated debris beds.

This report is directed towards development of a model to characterize the heat removal from superheated debris beds.

3. EXPERIMENTAL APPARATUS AND PROCEDURE

3.1 Description of Test Apparatus

An experimental facility was designed to study the characteristics of superheated spheres as they are either:

(i) quenched during fall through a pool of water and as they are subsequently cooled in a packed bed configuration, or

(ii) quenched while in a packed bed configuration only, by an overlying pool of water.

The experiment was designed to provide conditions of constant pressure boiling. This report focuses on case (ii). The apparatus used in the transient debris bed cooling experiments is described below.

Figure 3.1 presents a photographic view and a schematic diagram of the test apparatus. The basic systems of the apparatus are:

(i) heaters for establishment of initial sphere temperature, for preheating the test section wall and for heating the water;

(ii) a sliding gate shutter and actuation electronics and hydraulics;

(iii) test container;

(iv) test instrumentation;

(v) data acquisition and recording devices.

These systems are discussed individually below.

3.1.1 Heating Systems

The spheres are heated in a stainless steel container which is positioned in the furnace shown in Fig. 3.1(a). A schematic representation of the heating arrangement is shown in Fig. 3.1(b). Air delivered from a compressor flows through two high power density electrical resistance heaters, each rated at 2.4 kW, and connected in series. The hot air is directed to the furnace. The hot air stream flows past the spheres, heating them by forced convection. In addition, the oven itself is heated. The oven is rated at 4 kW and the oven temperature can be raised to 982 K. The air stream can be heated in the resistance heaters to an outlet temperature to approximately 871-982 K. The sphere temperatures are adjusted by a combination of air flow rate and temperature, and oven power level. This combination of heating techniques was found to be optimal in terms of providing sphere temperature uniformity.

A heating system was designed to preheat the test section wall to the desired temperature prior to an experimental run. The active portion of the test

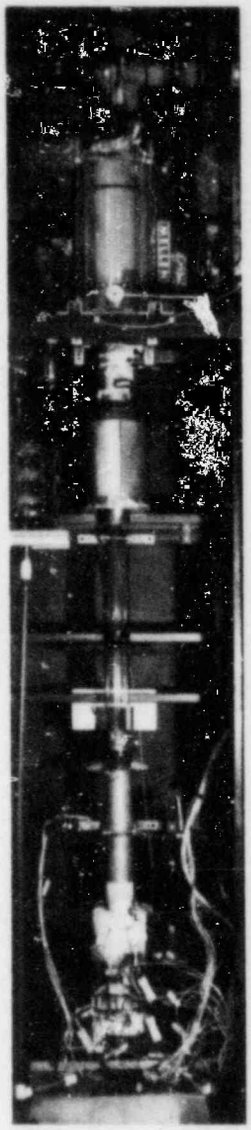

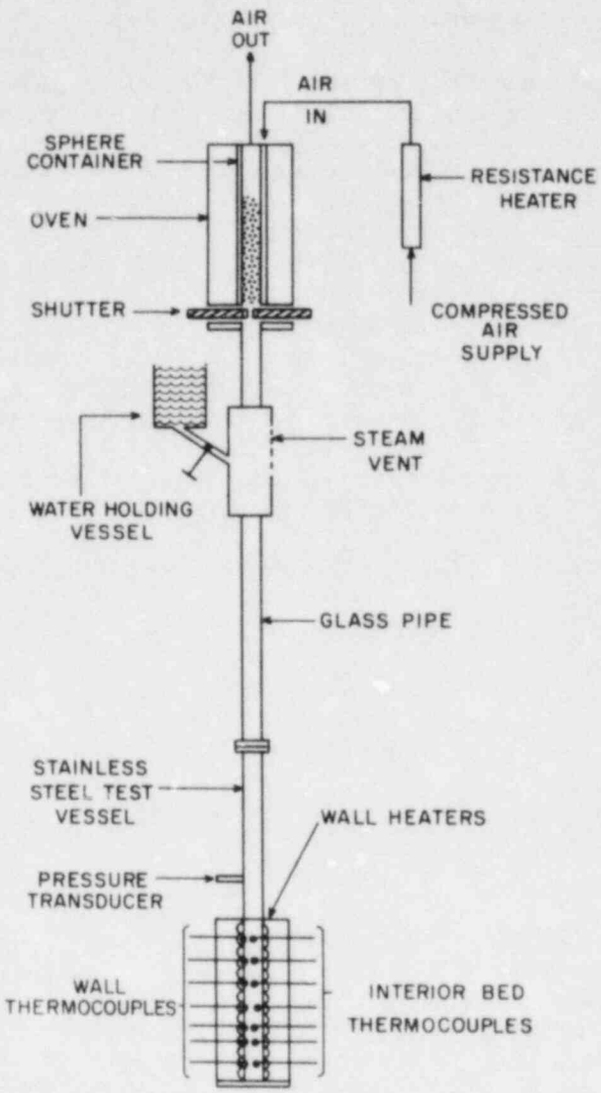

(a) (b)

FIG. 3.1 Photographic View of Test Apparatus:
(a) Photographic View
(b) Schematic View

vessel is wrapped with Nichrome heater wire. Four independent powerstats are used, each of which can supply up to 0.7 kW to the heaters.

3.1.2 Shutter System

While in the oven, the particles rest on a sliding gate shutter. The shutter plates are connected to compressed air-powered, spring-loaded pistons. An electrical impulse activates a solenoid valve to supply the pressure which drives the piston outward, thereby opening the shutter. This motion also compresses a spring on the cylinder. Upon relief of pressure, again by electrical signal actuation, the compressed spring drives the piston back and the shutter to its normally closed position. The open-close cycle can be chosen to be automatically timed, or can be operated manually. The shutter can be retracted completely from a closed position in approximately 50 milliseconds.

3.1.3 Instrumented Test Container

The test vessel shown in Fig. 3.1 is a Schedule 10 stainless steel pipe, 1.219 m long, 108.2 mm inside diameter, with a 3.05 mm wall thickness. It is closed at the bottom with a stainless steel flange which contains a drain port for draining water and removing the spheres. The pipe is coupled to a length of Pyrex glass pipe above it to permit visual observation of boiling in the pool of water above the particle bed.

The test section is instrumented with thermocouples which penetrate through the wall into the test container. The thermocouple junctions are located at the center of the pipe. Thermocouples are also mounted on the outer wall of the pipe. The vessel is wrapped to a height of 0.45 m with 20 gauge Lewis Engineering Heater wire, in order to preheat the test vessel wall.

3.1.4 Test Instrumentation

The test instrumentation includes:

(i) thermocouples in the oven to monitor and record sphere temperature,

(ii) a thermocouple to record initial water temperature,

(iii) thermocouples in the interior of the test container to record particle bed temperature and water pool temperature,

(iv) thermocouples on the test vessel wall,

(v) a pressure transducer mounted on the wall of the test vessel,

(vi) a shutter activation signal to record opening and closing of the shutter.

This instrumentation is discussed below. The data acquisition system is described following the instrumentation description.

Four thermocouples are used in the oven to monitor the sphere temperature distribution while heating is in progress. These temperatures are used to establish the sphere temperature initial condition. These sensors contain chromel-alumel grounded junctions with 3/16 inch diameter Inconel 600 sheaths. Limits of error on these thermocouples, specified by the manufacturer, are $\pm$ 2F for 32-530 F and $\pm$ 3/8% for 530-2300 F.

An additional thermocouple is used to measure water temperature prior to its release into the test vessel.

The test section instrumentation is shown schematically in Fig. 3.2. Swagelok fittings are mounted in a staggered fashion on the wall of the vessel to permit penetration of thermocouples to the interior. These thermocouples are used to monitor particle bed temperatures and water temperature above the bed. All of these thermocouples are exposed junction chromel-alumel sensors. They are 3.18 mm (1/8 inch) diameter, stainless steel sheathed elements. In practice, as is shown in Chapter 4, these thermocouples primarily provide an indication of the availability of water at the position of the sensor. The wall thermocouples are also chromel-alumel sensors whose junctions were flattened by impact and fastened to the outer wall of the test vessel.

One of the Swagelok fittings is used to mount a piezoelectric pressure transducer to the wall of the test vessel. This sensor is used to measure pressure fluctuations in the two-phase pool above the particle bed. This signal is used to identify the times of initiation and termination of boiling within the test vessel.

The shutter actuation system provides a d.c. output signal which indicates shutter actuation and closure times.

3.1.5 Data Acquisition and Recording

Table 3.1 summarizes all the data recording channels used in the experiments reported here. All of the data channels are routed to a Hewlett-Packard Model 21MX Data Acquisition System. Two data acquisition devices are used. A Hewlett-Packard Model 3495 Scanner in combination with a Model 3455A Digital Voltmeter, and a Neff System 620, Series 100 Amplifier/Multiplexer. Both systems have integral analog-to-digital converters. The scanner was used to record sphere and water initial temperatures. The Neff system was used to record all events during the transients. Data recording speeds of up to 50 kHz are possible with the Neff system. In these experiments a 1 kHz filter was used to remove high frequency noise, and the 16 available channels were sampled at a rate of 20 channels per second. The digital output from both devices was temporarily stored on disc memory and was transferred to magnetic tape at experimental run termination.

Subsequent to each run, the magnetic tape was played back using suitable software and the signals were plotted on paper.

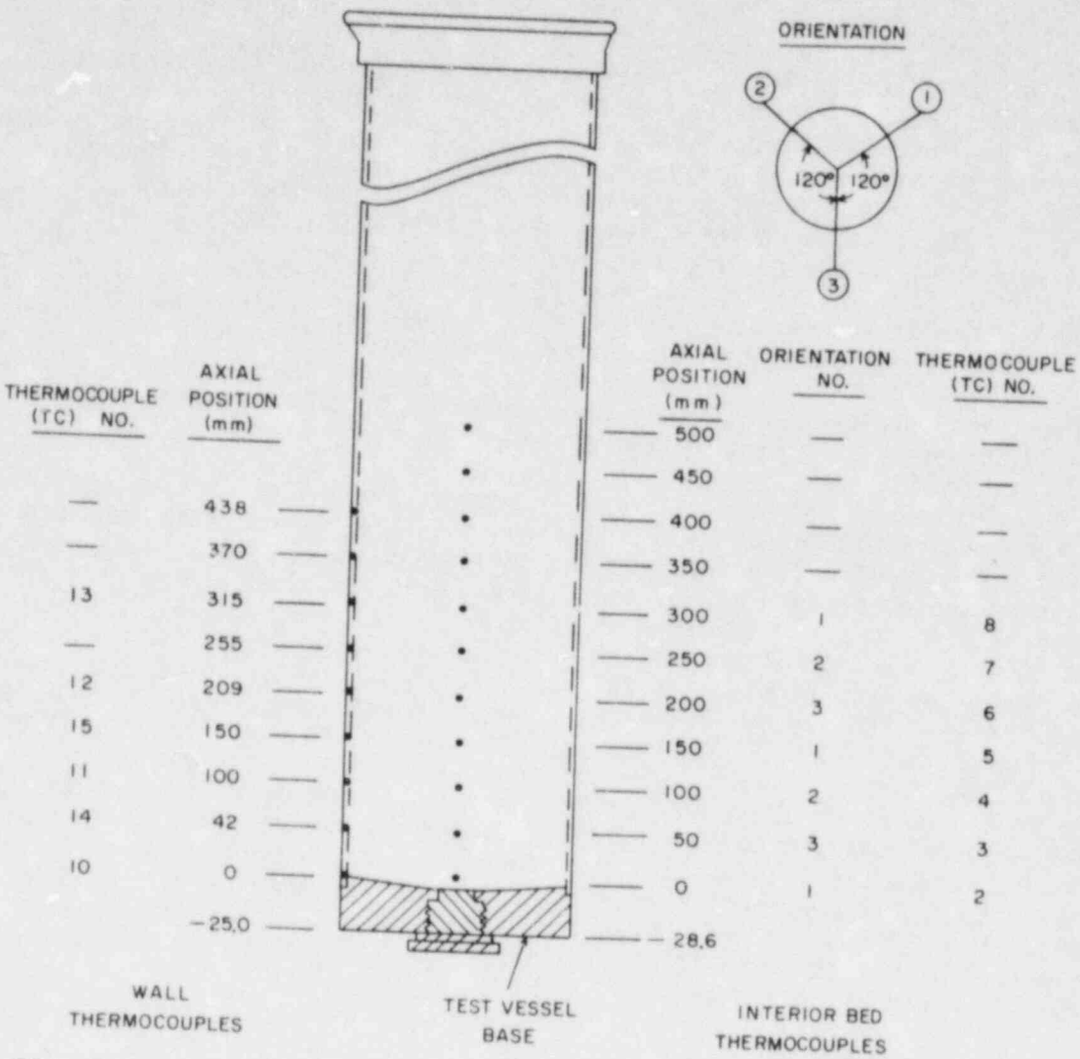

FIG. 3.2 Schematic Diagram of Test Vessel Instrumentation Positions

TABLE 3.1
Data Channels

Data	Channel Nos.
Shutter Signal	0
Pressure Transducer	1
Bed Thermocouples	2-8
Wall Thermocouples	10-15

3.2 Test Procedure

Prior to an experiment, a prescribed mass of spheres is measured out, loaded into the oven, and heated to the desired temperature. The sphere temperature distribution is monitored to assure heating uniformity. The measured temperature variation at a nominal sphere temperature of 533 K is approximately ± 10 K. For spheres heated to 977 K, the temperature variation is typically ± 20 K. Heating the spheres (15 kg typically) generally takes 2-4 hours, depending on the desired temperature.

While the spheres are heating, a selected mass of water is measured out and is heated (or cooled) to the desired temperature. In addition, the test section wall is heated to the prescribed temperature. Several of the wall temperatures are monitored on a strip-chart recorder prior to a run in order to allow adjustment of the temperature distribution along the wall.

An experimental run is initiated as soon as the initial sphere, water and wall temperatures are established. The water is then loaded into the water holding vessel. At this point, the shutter mechanism is activated by pressurization of the compressed air system. A computer data acquisition program is brought up on a computer terminal adjacent to the apparatus. This program first records the initial sphere and water temperatures, using the scanner system. Transient data acquisition is then initiated for a selected data sampling time interval. The shutter release mechanism is actuated and the spheres are dropped into the (dry) vessel, where they form a packed particle bed. All power, to the test apparatus, oven and test section wall, is turned off. A 30-60 second wait period is allowed for the bed thermocouples to heat to the sphere temperatures. After this wait period, the water is released from the holding vessel and flows into the test container and on to the bed of particles. Data acquisition continues for the duration of the preset sampling time period. This time period is chosen to assure data collection well beyond termination of boiling activity in the test vessel. The experiment is terminated at the end of the data sample period.

3.3 Test Parameters

Table 3.2 summarizes the range of experimental parameters considered thus far in this study. The conditions and parameters characteristic of each experimental run are listed in Chapter 4.

TABLE 3.2

Test Parameter Ranges

Parameter	Range
Packed Bed Particles	3 mm (± 0.25 mm) spheres
Particle Material	302 stainless steel
Bed Diameter	108.2 mm (test vessel i.d.)
Mass Particles	10-20 kg
Mass Water	8 -14 kg
Particle Temperature	533 K - 972 K (500 F-1300 F)
Water Temperature	274 K - 360 K
Particle Bed Height	218 - 433 mm

4. PARTICLE BED QUENCHING EXPERIMENTAL RESULTS

4.1 Experimental Run Parameters

Table 4.1 presents the run parameters of the packed particle bed quenching experiments. All experiments were performed using 3.18 mm diameter 302 stainless steel spherical particles. The sphere temperatures listed in Table 4.1 represent the average of four temperatures from thermocouples distributed within the particle container in the furnace described in Section 3.1.1. The test vessel wall was heated to the initial sphere temperature in all cases but those indicated by asterisks.

The particle bed porosity was not measured during the quenching experiments. The porosity was measured, however, in separate effects tests with spheres at room temperature. These tests indicate that the bed porosity was in the range 0.35 - 0.40.

4.2 Characteristic Qualitative Features of Results

The range of parameters considered in the experiments listed in Table 4.1 has led to a spectrum of observations which, to some extent, depend on specific conditions. The results, however, have some qualitative features in common. Therefore, before discussing the differences in behavior which depend on specific conditions, a "representative" experimental run is considered in detail. The data are presented and features of the data are discussed.

Consider Run No. 116, the initial conditions of which are listed in Table 4.1. The sphere and wall temperatures are both 818 K (nominally 1000 F) for this run. Figures 4.1(a)-(d) presents the data for this experiment. Figure 4.1(a) is a plot of the shutter actuation signal and the pressure transducer trace. Figures 4.1(b) and (c) show the particle bed temperatures on two different scales. The wall temperature traces are shown in Fig. 4.1(d). In these and all such subsequent plots, zero time corresponds to the initiation of data acquisition.

Figure 4.1(a) indicates that the shutter was opened at approximately 5 seconds after data acquisition was initiated, at which time the spheres were dropped into the test vessel. The bed thermocouples, which were initially heated by conduction from the hot walls of the vessel, began to respond to the surrounding hot spheres at approximately 5 seconds. These thermocouples were allowed about 30 seconds to equilibrate to the sphere temperature, after which the water was released on to the spheres. The pressure transducer shows a first indication of activity at 38.6 seconds, while thermocouple (TC) number 8 (TC8) responded to the presence of water at 39.5 seconds.

The outstanding feature of Figs. 4.1(b) and (c) is the sequence of step changes in temperatures, beginning with TC8 located near the top of the bed. This sequence then proceeded in the downward direction to each thermocouple in the bed. The temperature at each position suddenly fell from the initial sphere temperature to the liquid saturation temperature. The thermocouples read nearly constant temperature until a step change occurred. The initial

TABLE 4.1

Experimental Run Parameters

Run Number	Sphere Temperature T_o (K)	Water Temperature (K)	$T_o - T_{SAT}$ (K)	Mass Spheres (kg)	Mass Water (kg)	Bed Height (mm)
107	537.0	356	164.0	15.	8	327
108	538.3	362	165.3	15.	8	327
109	535.3	296	162.3	15.	8	327
110*	538.5	297	165.5	15.	8	327
111	814.3	296	441.3	15.	8	327
112	817.0	298	444.0	15.	8	327
113*	820.0	298	447.0	15.	8	327
114*	821.8	364	448.8	15.	8	327
115	808.5	362	435.5	15.	8	327
116	818.0	361	445.0	15.	8	327
117	537.3	294	164.3	15.	8	327
118	536.5	274	163.5	15.	12	327
119	815.8	274	442.8	15.	14	327
120	535.0	363	162.0	15.	8	327
121	534.3	274	161.3	15.	12	327
123	971.8	364	599.8	14.1	12	307
124	538.0	274	165.0	15.	12	327
125	540.0	276	167.0	15.	8	327
126	816.3	364	443.3	15.	8	327
127	682.8	363	309.8	15.	8	327
128	674.0	364	301.0	15.	8	327
129	815.3	361	442.3	15.	8	327
130	672.3	362	299.3	15.	8	327
132	808.0	361	435.0	20.	12	433
133	820.8	355	447.8	10.	8	218

*Test vessel wall initially at room temperature

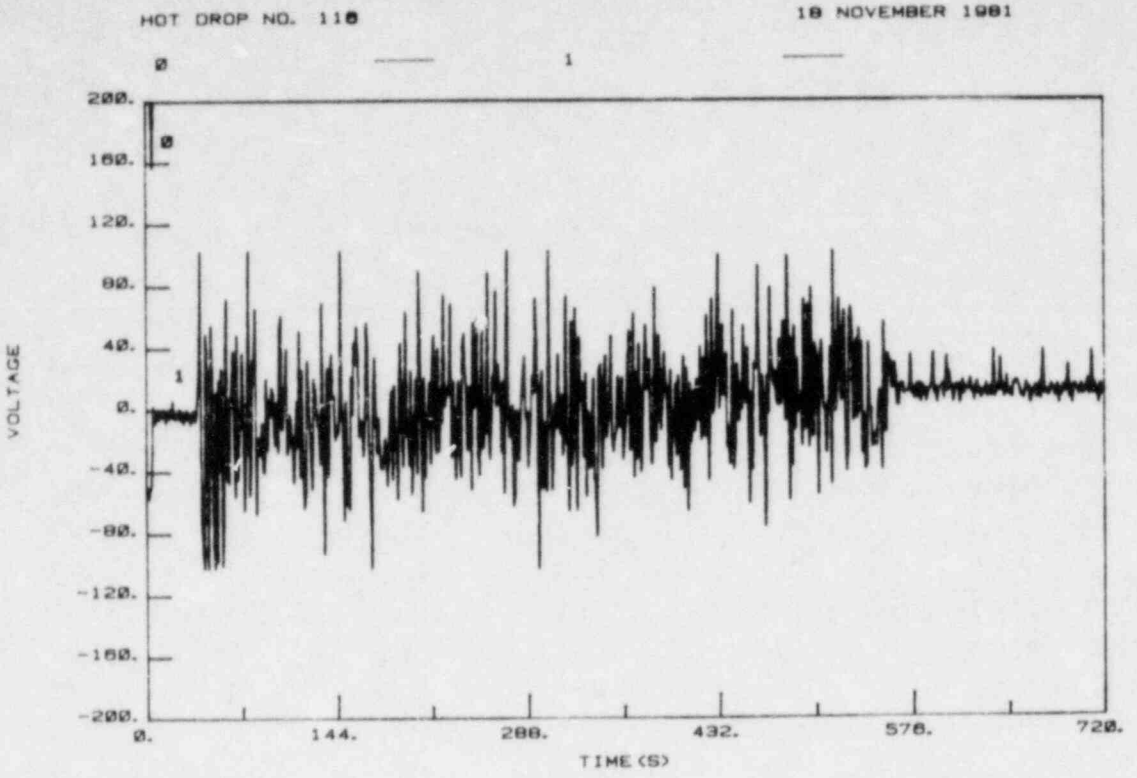

(a) Shutter and Pressure Transducer Signals

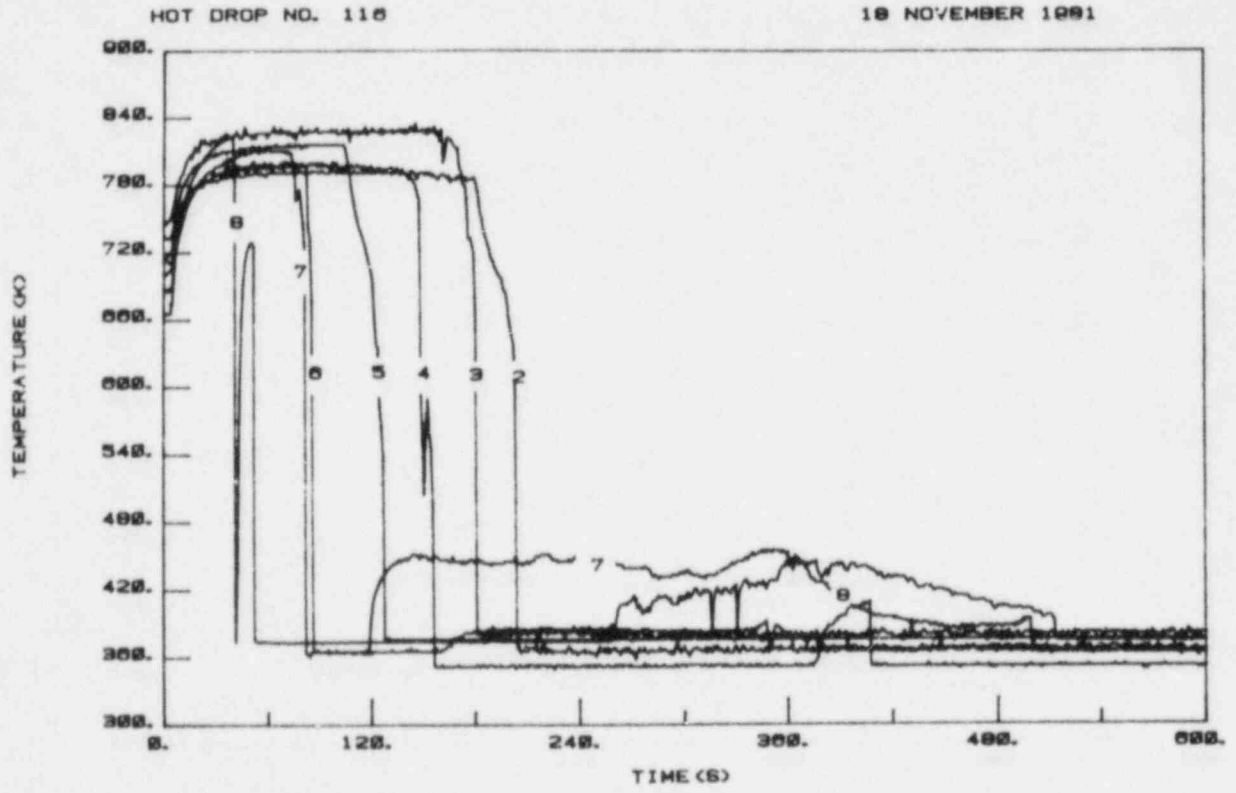

(b) Temperature Traces - Entire Time

FIG. 4.1 Results of Run No. 116

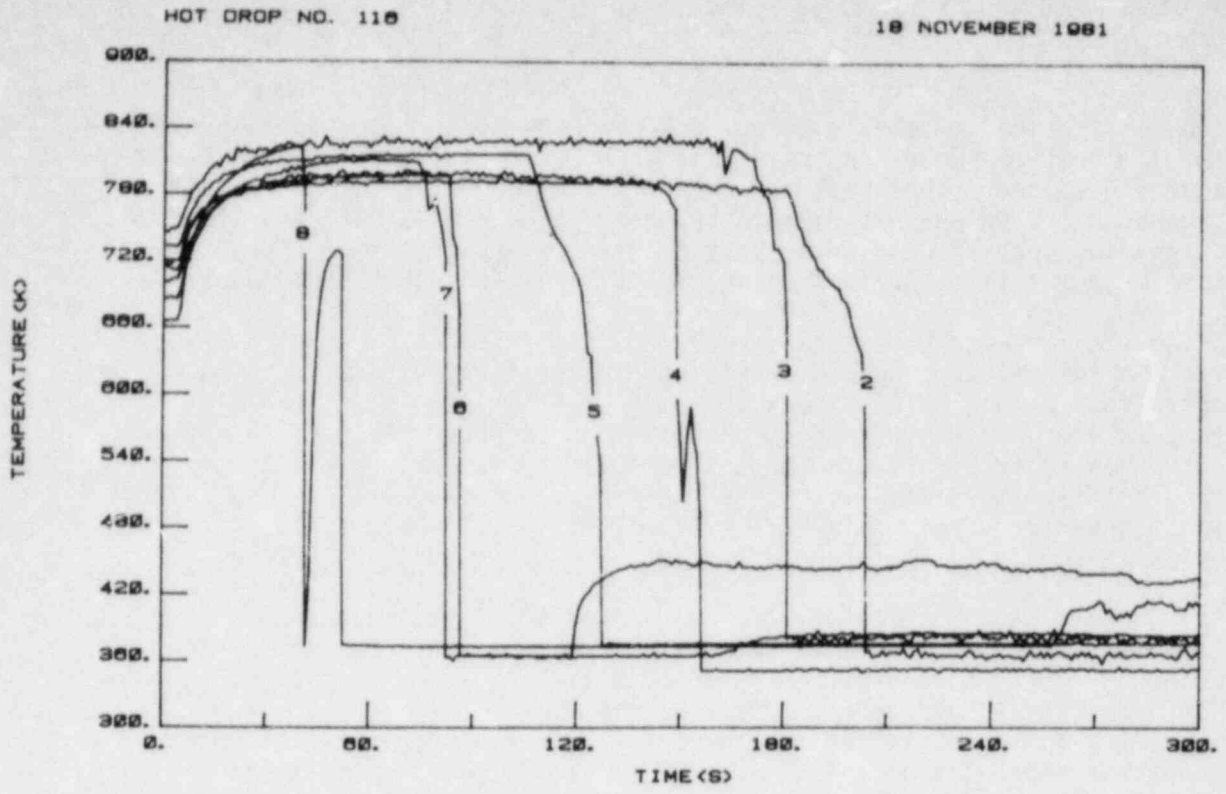

(c) Temperature Traces - Expanded Scale

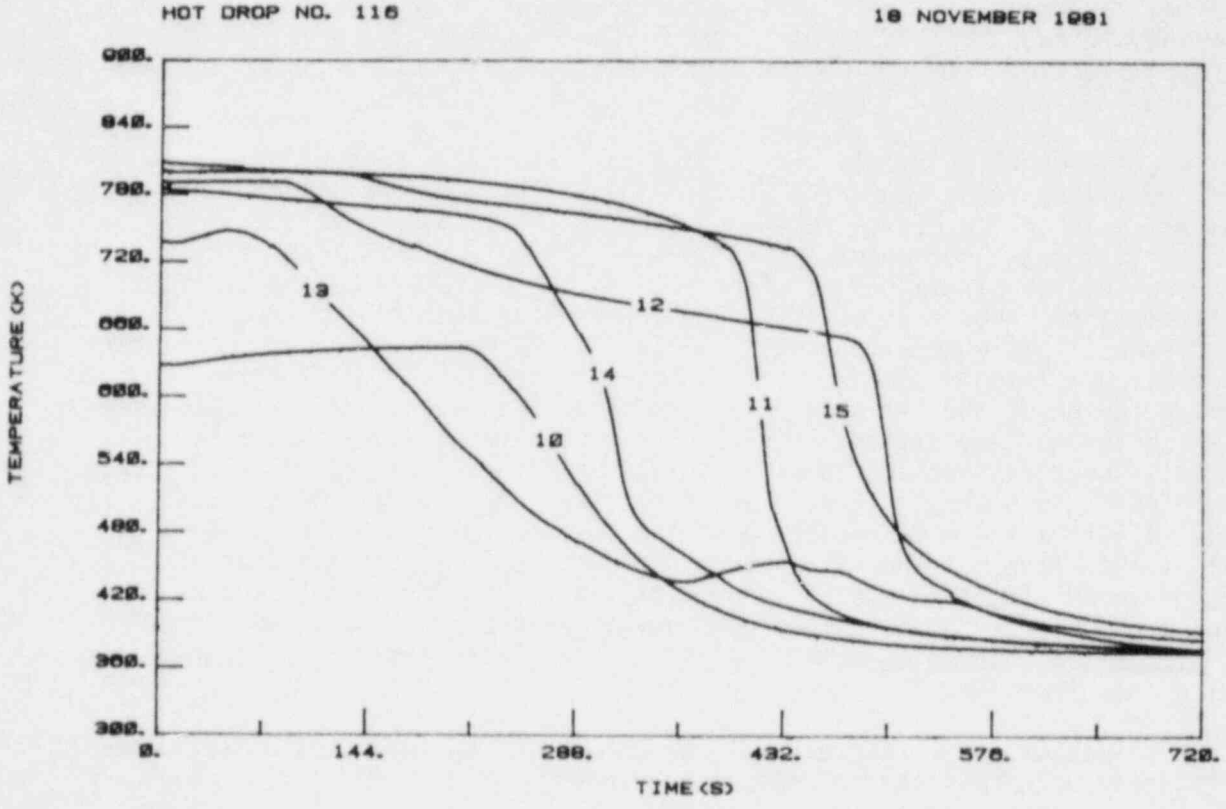

(d) Wall Temperatures

FIG. 4.1 Results of Run No. 116

drop in temperature is usually observed to be very sharp. This sequential pattern of temperature reduction is indicative of a frontal cooling behavior which propagates down the column. It is a characteristic feature of nearly all of the data acquired in the experiments reported here. It is believed (further discussion is found in Chapter 5) that the sudden drop in temperature is indicative of the first arrival of water to the site of the thermocouple.

Figure 4.1(b) indicates that several of the thermocouples partially recover their initial temperature subsequent to the first arrival of liquid. In this case four channels (TC Nos. 4, 6, 7, 8) exhibit this behavior. The temperature recovery characteristic of Run No. 116 occurred in many, though not all, of the experiments. In some runs more of the thermocouples showed recovery, while in other runs all of the thermocouples recovered to nearly their initial temperatures. This feature of the results will be discussed in subsequent sections.

At 500 seconds, Fig. 4.1(b) indicates that TC8 is quenched, i.e., its temperature is reduced to the liquid saturation temperature. No subsequent thermocouple reheat is observed. This suggests that the particle bed is completely quenched at this point. The pressure transducer, however, indicates boiling activity to 565 seconds. Figure 4.1(d), which presents the outer wall surface temperatures, suggests that the final boiling activity in the test vessel is due to quenching of the test vessel wall. The pressure transducer indicates boiling took place in the test vessel for 527 seconds.

A sequential pattern of wall quenching is observed in Fig. 4.1(d). The first wall thermocouple to indicate significant wall cooling is TC13, located above the bed (see Fig. 3.3). Aside from TC13, however, the sequence of quenching proceeds from the bottom thermocouple, TC10, to the top of the bed at TC12.

Three "frontal" particle bed cooling patterns are suggested by Figs. 4.1(b)-(d). The first, observed in Fig. 4.1(b), is a downward-progressing front which is interpreted as being related to the first arrival of liquid to the site of the thermocouples. The times of arrival of this front to each of the thermocouples can be deduced from Fig. 4.1(b) by observing the departure of the temperatures from the nearly horizontal initial temperature lines. A second frontal pattern is suggested by Fig. 4.1(b) but is not quite convincingly displayed. This is a sequence of an upward-propagating front which leads to final quenching of the thermocouples. Additional data are presented in Section 4.4 which further support the existence of such a front under some circumstances. The times associated with arrival of such a front can also be picked off the abscissa of Fig. 4.1(b). The third frontal pattern, suggested by Fig. 4.1(d) is associated with quenching of the test vessel wall. The time of arrival of this front at the wall thermocouple sites is associated with the "knee" in each of the curves plotted in Fig. 4.1(d) which is followed by the steepest drop in temperature for each curve. This rapid drop in wall temperature is believed to be associated with the transition from film to nucleate boiling heat transfer.

The times of arrival of each of the three cooling fronts as a function of axial position in the test column are presented in Fig. 4.2. Time in all

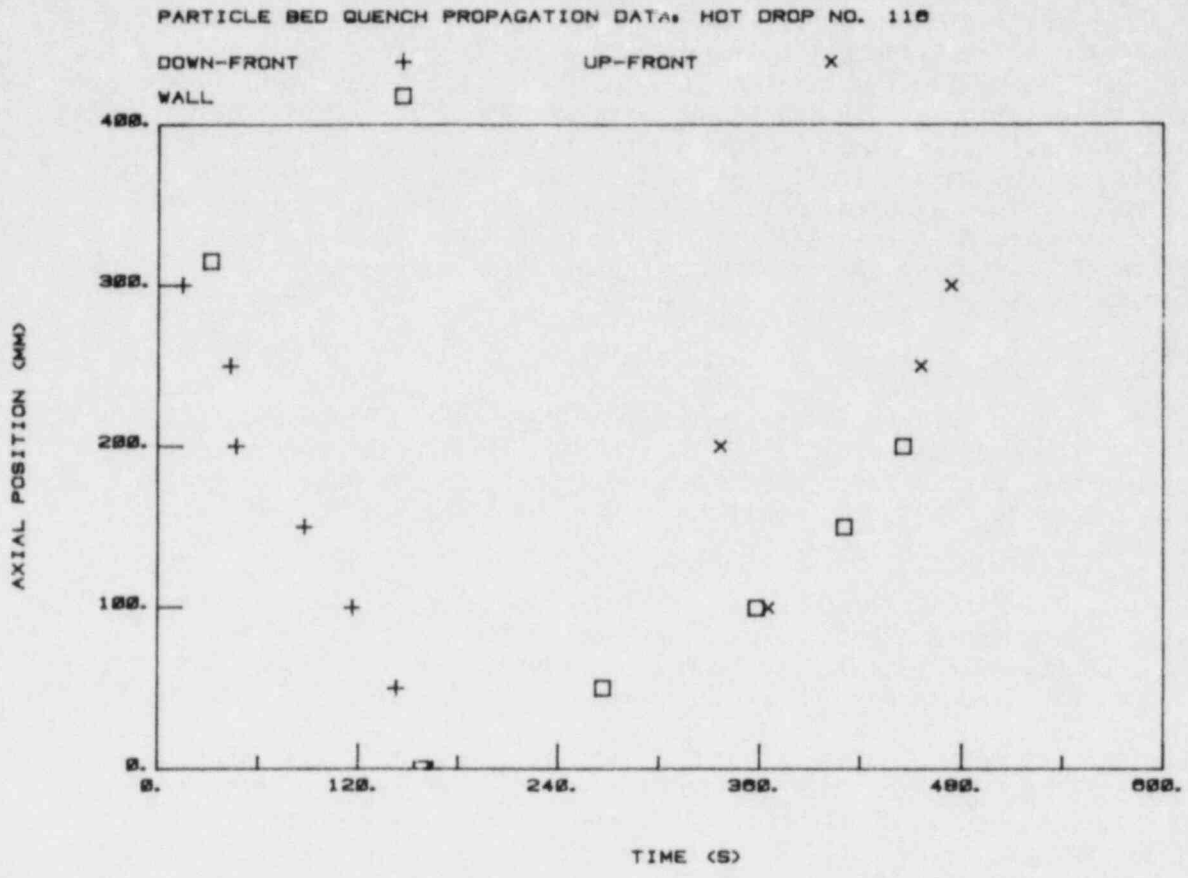

FIG. 4.2 Frontal Propagation Results: Run No. 116

frontal propagation plots of this type is measured from initial water-sphere contact time, which is deduced from the pressure transducer response traces. This front propagation data summarizes the observations discussed above. Figure 4.2 shows the advance of the downward-propagating front which reaches the bottom of the bed at 165 seconds. At this point an upward-propagating front is observed which is responsible for "final" cooling of the thermocouples within the particle bed as well as the vessel wall.

The position vs. time curve for the downward-propagating front in Fig. 4.2 appears to follow a linear trend. A least-squares analysis on these data yields a propagation speed of 1.92 mm/s. The behavior of the "up-front" is more complex. A least-squares analysis of the "wall" data gives a propagation speed of 0.69 mm/s. An insufficient number of points are available to perform a similar calculation on the "up-front" data of Fig. 4.2. Taking the wall and up-front data points together (and excluding the wall point at 250 mm and up-front point at 200 mm), a least-squares analysis leads to a propagation speed of 0.87 mm/s. It is a characteristic feature of the data that the upward-directed front speed is less than the downward-directed speed. A more detailed discussion of front propagation speeds is presented in Section 4.7, and of heat transfer rates in Section 4.8.

4.3 Effect of Test Container Wall Temperature

A series of experiments was performed to determine the effect of wall temperature on the mode of particle bed quenching. These tests were conducted as a consequence of preliminary experiments (Ginsberg, 1981), which suggested that the wall temperature boundary condition could drastically affect the mode of bed cooling.

Run No. 114 was performed under the same nominal conditions as Run No. 116 discussed above, except that the wall was not heated prior to the test. The wall, therefore, was initially at room temperature. The results of this test series are presented in Figs. 4.3(a) and (b).

The spheres were dropped into the vessel at approximately 10 seconds following initiation of data acquisition. The pressure transducer indicates water contact with the bed at 38 seconds. TC8, the uppermost thermocouple in the bed, shows two cycles of cooling and reheating before finally remaining at elevated temperature until the final quench. Following TC8, the next thermocouple to show contact with water is TC2, the one closest to the base of the test column. From the time that TC2 shows water contact, the remaining thermocouples sequentially quench from the bottom upwards, i.e., from TC2 at the bottom to TC8 at the top. In this experiment there was no evidence of a downward-directed cooling front. The mode of particle bed quenching suggested by the data is via an upward-propagating cooling front. This behavior is in marked contrast to that observed in Run No. 116 and discussed in Section 4.2. Figure 4.4 summarizes the frontal behavior discussed above.

All of the experimental runs listed in Table 4.1 with unheated test vessel wall exhibited the upward-propagating cooling front behavior discussed above. None of these runs exhibited the early downward progression of liquid as discussed in Section 4.2. This result is interpreted to imply that while the

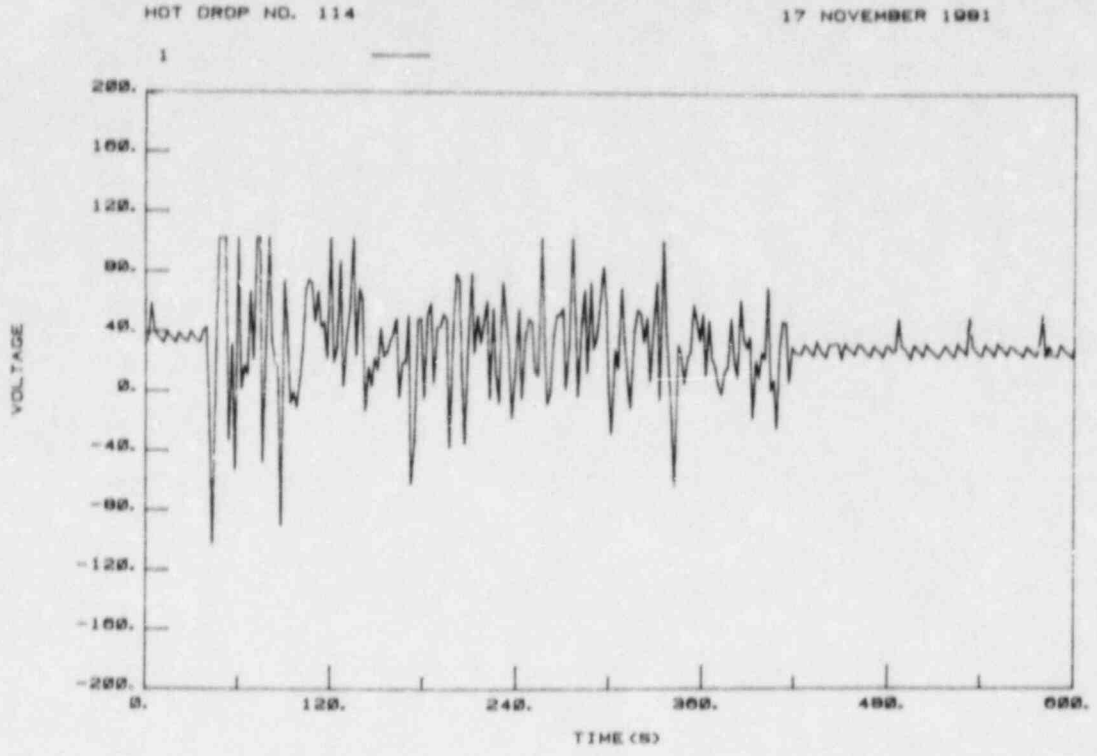

(a)

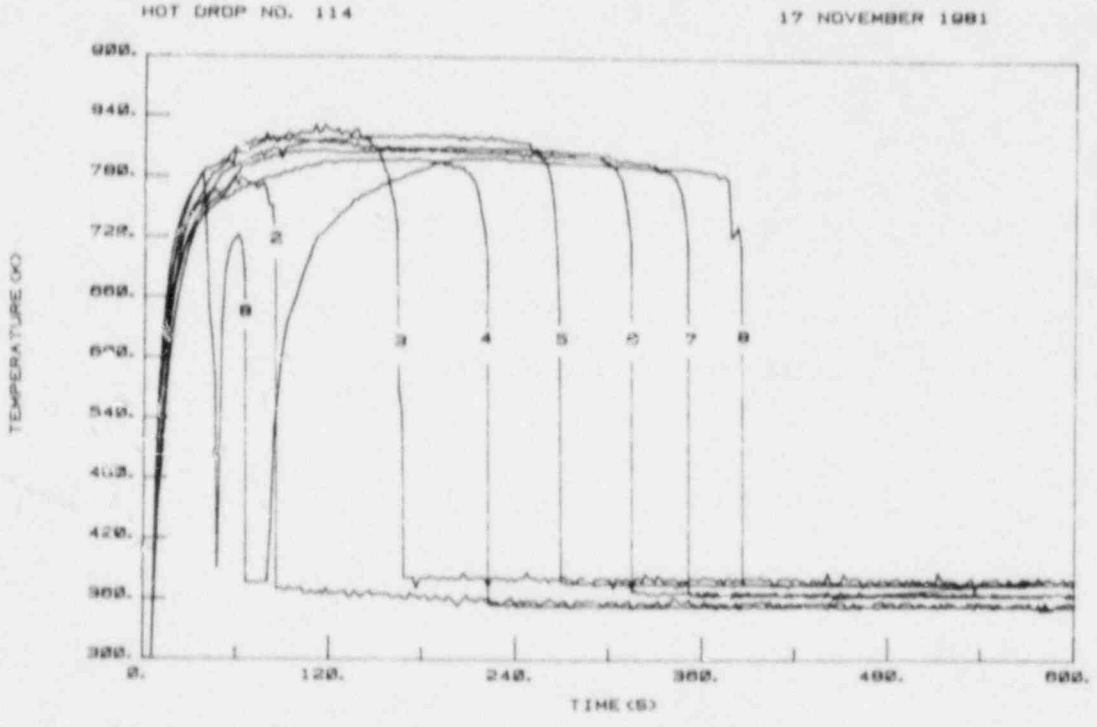

(b)

FIG. 4.3 Results of Run No. 114: (a) Pressure Transducer Signal; (b) Temperature Traces

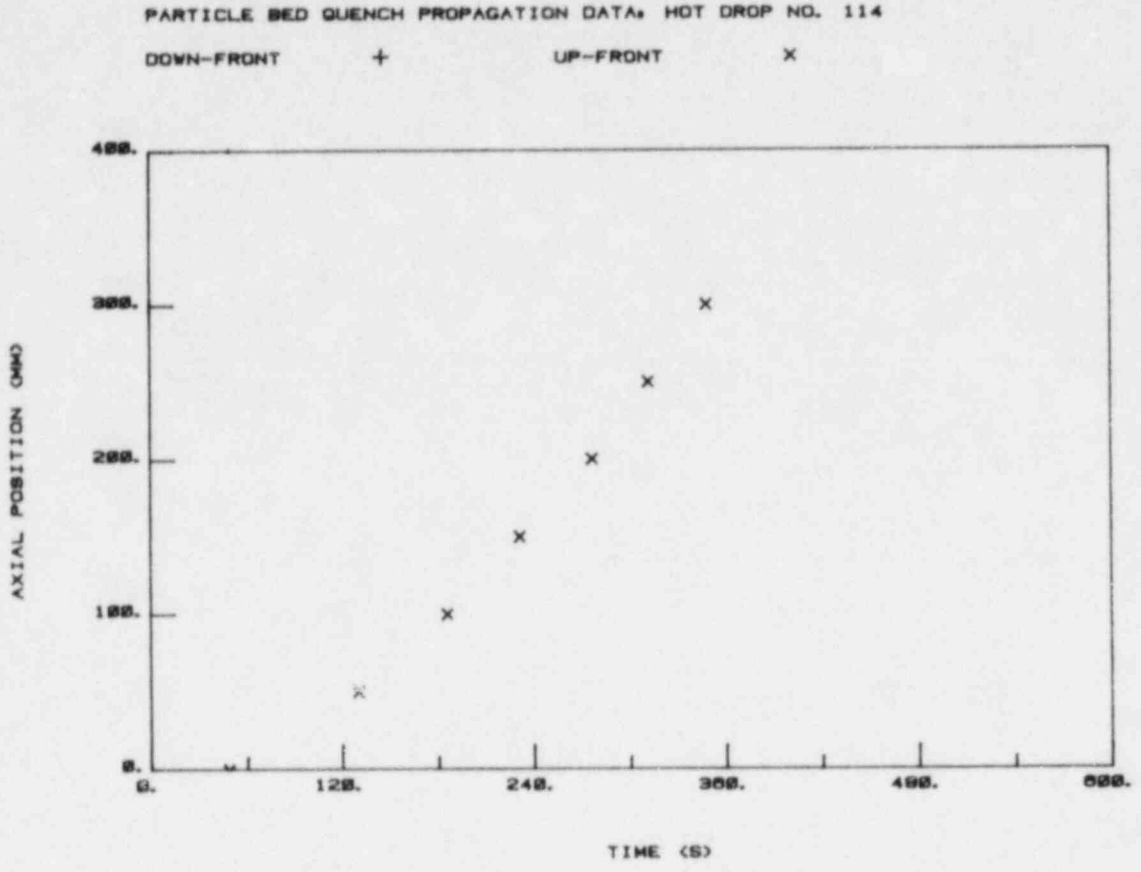

FIG. 4.4 Frontal Propagation Results: Run No. 114

water began to penetrate the bed from the top downward, liquid subsequently bypassed the central portion of the bed (where the bed thermocouples were located) and flowed to the base of the column along the outer perimeter of the bed adjacent to the vessel wall. The initial downward-propagating cooling frontal motion was arrested and bed cooling then proceeded in the upward direction.

The interpretation of these results is discussed in Chapter 5. To summarize, however, it was concluded that the behavior characterized above was caused by the presence of the cold vessel wall. The experiment was designed to simulate a large debris bed where the influence of bounding walls would be minimal. In the small-scale simulation experiments performed here, the wall condition was designed to simulate, as closely as possible, layer of particles. It was decided, therefore, to conduct all experiments with identical wall and sphere initial conditions.

4.4 Data Reproducibility

Experiments 116, 126 and 129 were performed under nominally identical conditions, as indicated in Table 4.1. The results of Run Nos. 126 and 129 are presented in Figs. 4.5 and 4.6, while those of No. 116 are shown in Fig. 4.1.

The temperature traces all show the characteristic sequential pattern of temperature drop, beginning at the top of the bed and proceeding downward. The only major deviation from this pattern is that of TC8 of Run No. 126 in Fig. 4.5. The response of this thermocouple is distinctly slower than the others.

The downward frontal behavior is represented for each run in Figs. 4.1, 4.5 and 4.6. Table 4.2 presents the downward propagation speeds which, in general, lie within ± 10% of each other. The scatter in this data has been found to decrease as the initial sphere temperature increases. This will be discussed in further detail in Section 4.8.

The major noticeable distinction between Runs 116, 126 and 129 is the extent of thermocouple temperature recovery following passage of the downward-propagating front. In Run 129 only one thermocouple recovers. TC6 in this case shows a very small temperature increase, i.e., the temperature rise above saturation is small compared to initial sphere temperature difference ($T_0 - T_{SAT}$). All other thermocouples remain at saturation temperature after passage of the first front. Four of the thermocouples in Run 116 and 6 thermocouples in Run No. 126 show some degree of recovery. The quench pattern of the thermocouples which show recovery indicates passage of an upward-moving front in Runs 116 and 126, which closely follows the quench of the test vessel wall. The wall quench frontal speeds for these cases are shown in Table 4.2.

The reproducibility of Experiments 116, 126 and 129 is typical of the data obtained thus far in the experimental program. The downward propagation cooling pattern is quite consistent and reasonably reproducible. The data indicate, however, that the thermocouples recover their temperature following passage of the downward-moving front in a manner that is not reproducible, either in number of thermocouples indicating this behavior or in magnitude of the temperature rise. Because of this lack of consistency, it is sometimes difficult

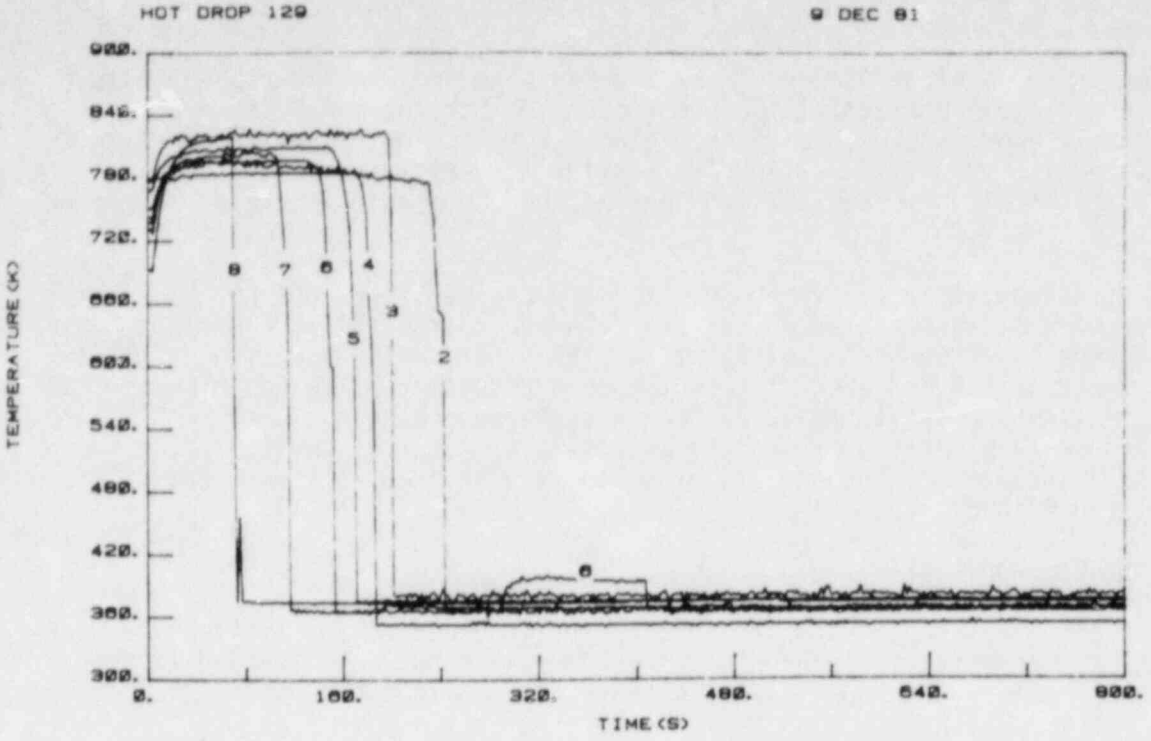

(a)

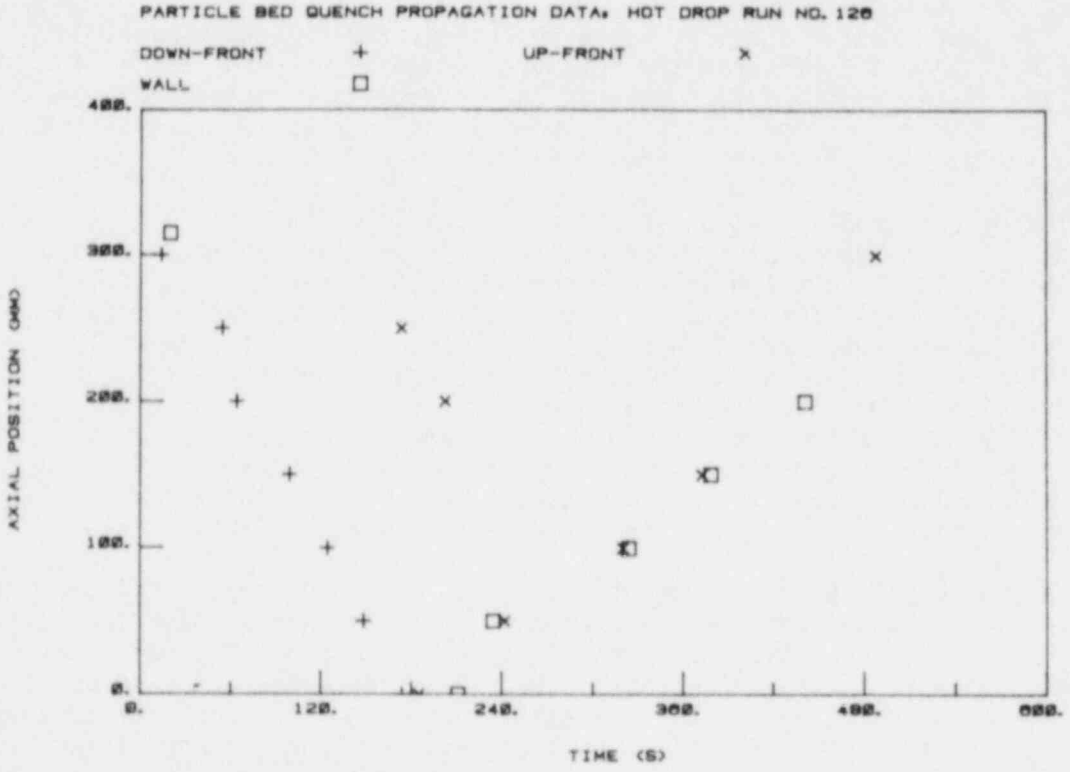

(b)

FIG. 4.5 Results of Run No. 126: (a) Temperature Traces; (b) Frontal Propagation Results

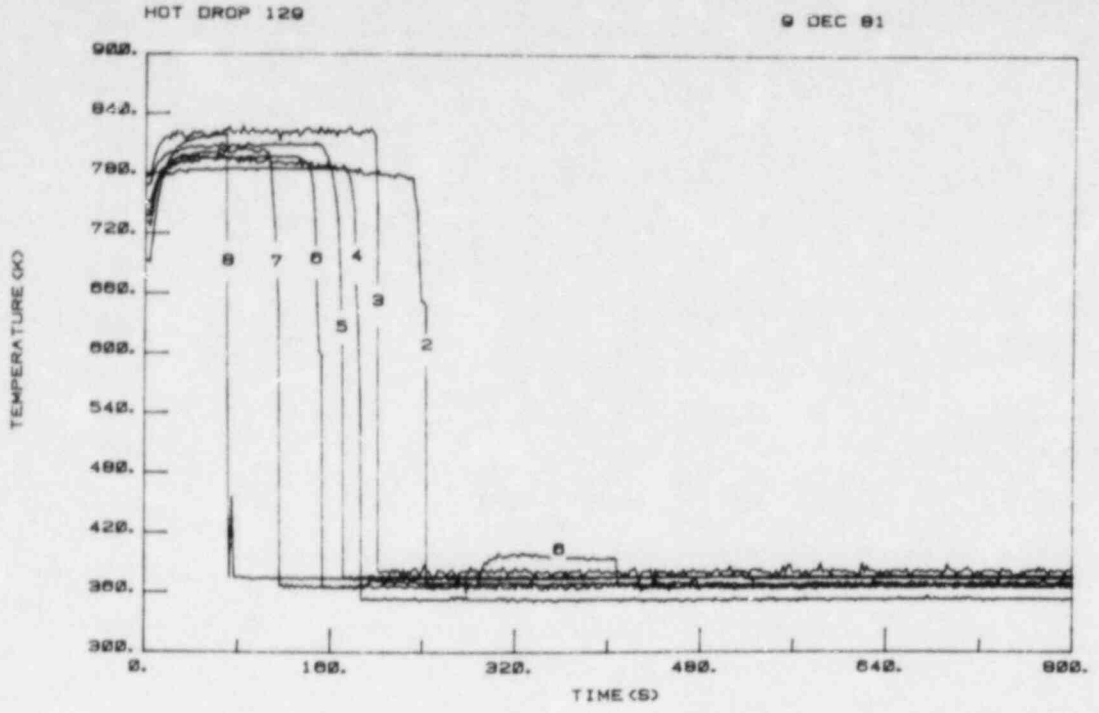

(a)

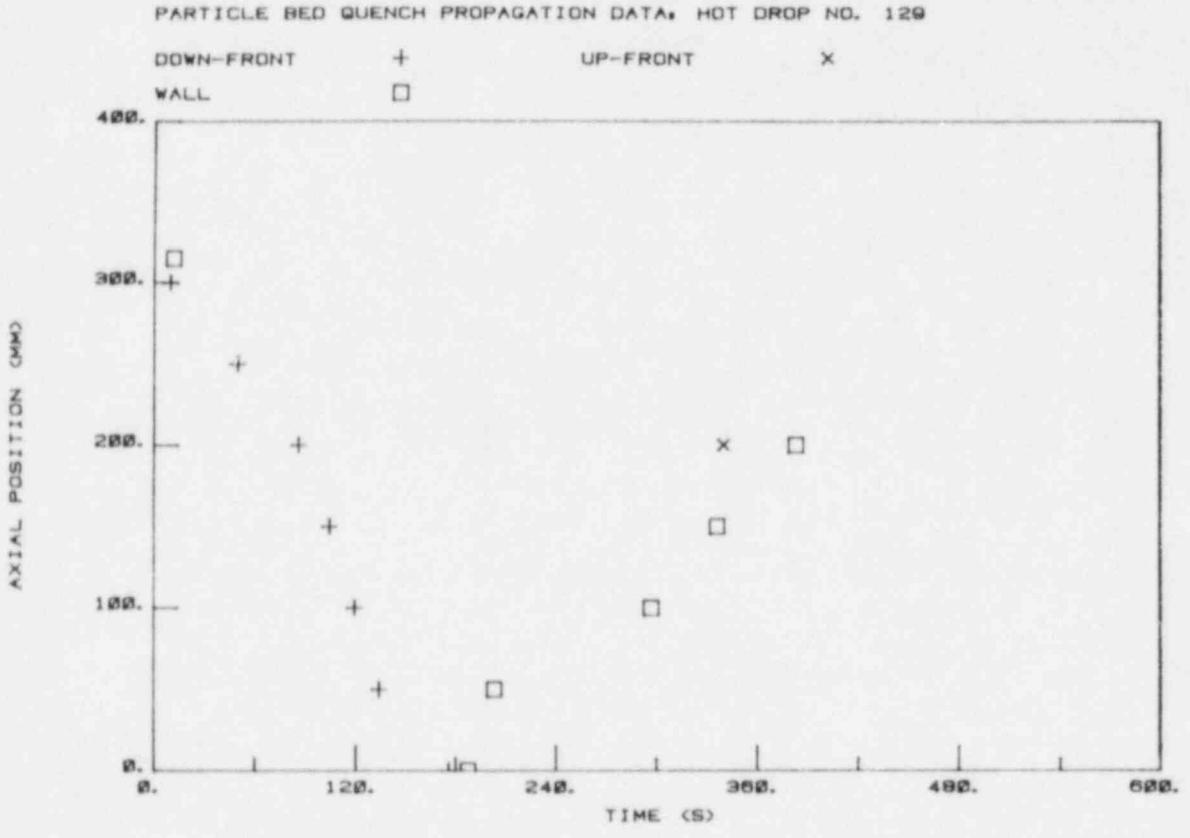

(b)

FIG. 4.6 Results of Run No. 129: (a) Temperature Traces; (b) Frontal Propagation Results

TABLE 4.2

Summary of Computed Time Scales, Propagation Speeds and Heat Fluxes*

Run No.	T_o-T_{SAT} (K)	t_d (s)	t_Q^{PT} (s)	t_Q^{TC} (s)	t_u (s)	v_d (mm/s)	v_u** (mm/s)	q''_{avg} (W/m^2)	q''_{max} (W/m^2)
107	164.0	44.4	189.6	193.9	149.5	6.55	1.92	$.82\times10^6$	3.57×10^6
108	165.3	43.9	217.9	204.3	166.4	7.09	1.97	.78	3.65
109	162.3	39.0	183.7	158.5	119.5	7.64	2.64	.99	4.03
110	165.5	8.9	131.7	118.9	110.0	--	2.27	1.34	--
111	441.3	154.0	507.9	455.1	301.1	2.22	--	.94	2.76
112	444.0	151.0	486.5	450.7	299.7	1.87	--	.95	2.83
113	447.0	41.9	375.8	367.3	325.4	--	0.77	1.18	--
114	448.8	48.3	379.1	365.9	317.6	--	1.01	1.19	--
115	435.5	160.6	558.5	472.7	312.0	1.96	--	.88	2.59
116	445.0	166.5	526.9	472.7	306.2	1.92	0.98	.90	2.57
117	164.3	39.5	155.1	160.0	120.5	7.65	--	.99	4.41
118	163.5	50.5	187.0	131.7	81.2	5.52	--	1.20	3.12
119	442.8	129.9	--	346.3	216.4	2.01	--	1.23	3.28
120	162.0	41.7	171.7	164.9	123.2	6.70	--	.95	3.74
121	161.3	33.8	144.4	121.9	88.1	8.46	3.72	1.27	4.59
123	599.8	230.3	640.0	535.6	305.6	1.41	--	1.01	2.35
124	165.0	34.1	142.4	121.0	86.9	8.70	--	1.32	4.67
125	167.0	44.7	151.5	128.6	83.9	6.03	--	1.25	3.60
126	443.3	175.7	521.0	487.0	311.3	1.91	0.40	.88	2.45
127	309.8	142.3	361.4	335.1	192.8	2.25	1.40	.89	2.10
128	301.0	119.2	--	--	--	2.77	--	--	--
129	442.3	174.4	487.8	382.5	208.1	1.94	--	1.11	2.44
130	299.3	108.5	354.1	324.8	216.3	3.09	--	.89	2.67
132	435.0	256.4	651.2	578.0	321.6	1.92	0.57	.97	2.19
133	447.8	95.4	350.3	299.0	203.6	2.07	--	.97	2.19

*Refer to Table 4.1 for experimental conditions

**Blanks indicate insufficient number of data points for least-squares analysis

to discern an upward-rising front from the bed thermocouples. These aspects of the data are discussed in Section 5.1.

4.5 Effect of Sphere Temperature

4.5.1 Temperature Trace Characteristics

This section focuses predominantly on the observed features of the temperature traces and their variation with initial sphere temperature. Some consideration, however, is given here to the quench front results. Section 4.5.2 examines the quench front results in more detail.

The effect of initial sphere temperature is examined by comparing Run Nos. 107, 127, 116 and 123. Except for the sphere initial temperature, these experiments were carried out under nominally identical conditions. As indicated in Table 4.1, the water temperature in thse runs was approximately 363 K, or 10 K subcooled. The temperature traces for Runs 107, 127 and 123 are presented in Figs. 4.7 - 4.9, together with the frontal progression results. The results for Run No. 116 are shown in Figs. 4.1 and 4.2.

With only one exception, the experimental results exhibit the downward-directed cooling front behavior. This behavior is indicated by the sequential sharp temperature drops exhibited by the bed thermocouples. This pattern is evident in the temperature traces of Figs. 4.1, 4.2, 4.7 and 4.9, and in their associated frontal propagation plots. The one exception to this behavior is shown in Fig. 4.8, which shows the results of Run No. 127. This run is discussed below in further detail.

Following the initial downward cooling progression, the data show that all runs exhibit some degree of temperature rise of the bed thermocouples. This temperature "recovery" suggests that, in all the runs discussed in this section, the initial downward-directed cooling front does not remove all of the stored sphere energy as it progresses down the particle bed. The magnitude of the observed temperature rise and the number of thermocouples which exhibit such a rise are not reproducible quantities, as discussed in Section 4.2. There is, however, a general trend discernable in the temperature traces which suggests that the extent of temperature recovery decreases as the initial sphere temperature increases. Thus, for an initial sphere temperature of 533 K nearly all the thermocouples represented in Fig. 4.7 show some degree of recovery. Furthermore, those that do recover remain at temperatures close to the initial sphere temperature until later in the transient. On the other hand, for an initial sphere temperature of 972 K, Fig. 4.9 shows only two thermocouples which recover. The magnitude of the recovered temperatures are smaller than tnose characteristic of, for example, Run No. 107 shown in Fig. 4.7 for the 533 K sphere temperature.

Particle bed quench propagation results were extracted from the temperature traces in the manner described in Section 4.2. The results are presented along with the temperature traces in Figs. 4.2 and 4.7-4.9. Data are shown for three frontal patterns: bed downward- and bed upward-propagation, and wall cooling. These figures display the discernable pattern of frontal cooling observed in the temperature traces. These data further suggest that the wall of the test vessel and the thermocouples within the particle bed were both finally quenched to the saturation temperature during the final upward-directed frontal

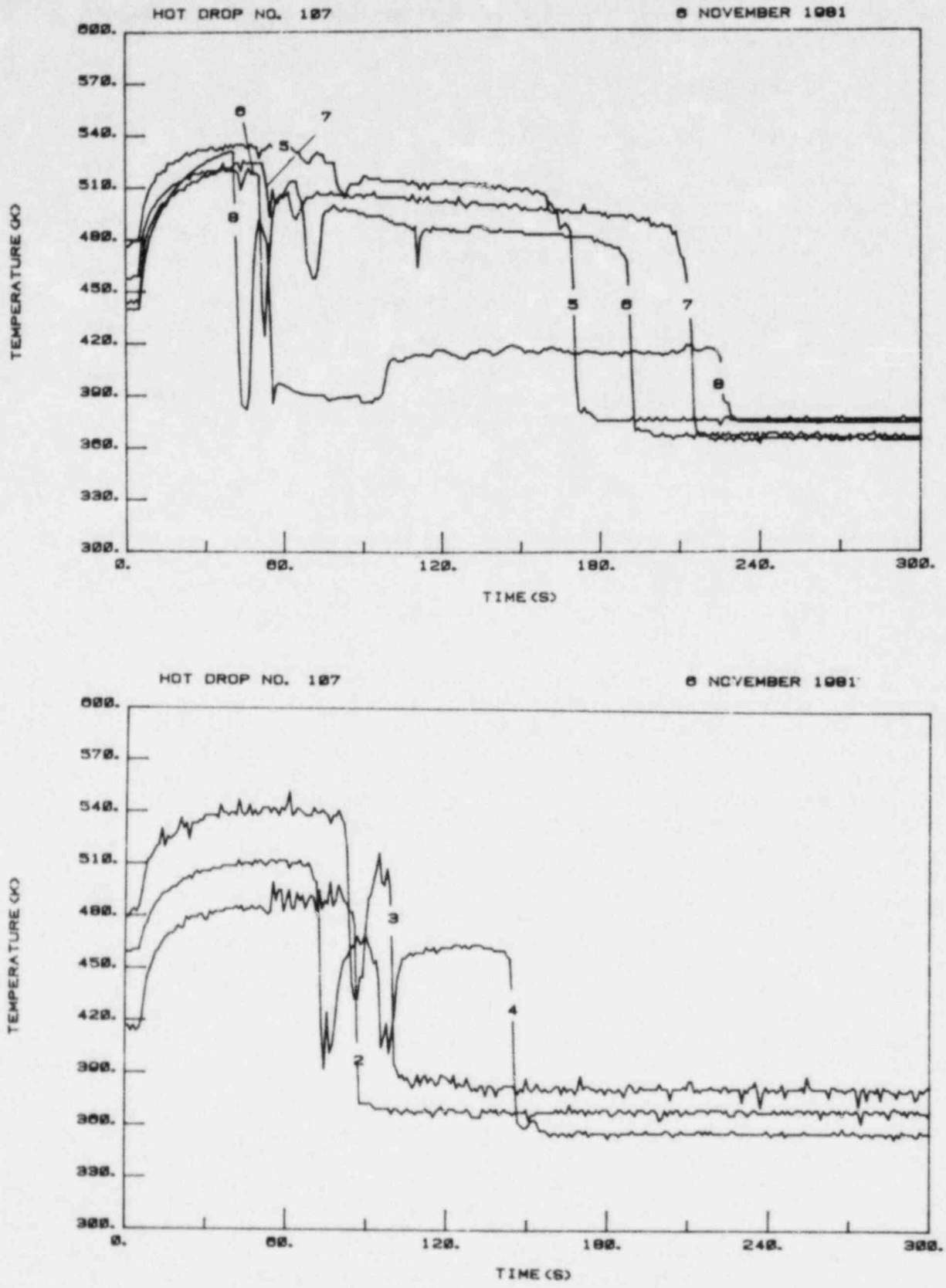

FIG. 4.7 Results of Run No. 107: Temperature Traces

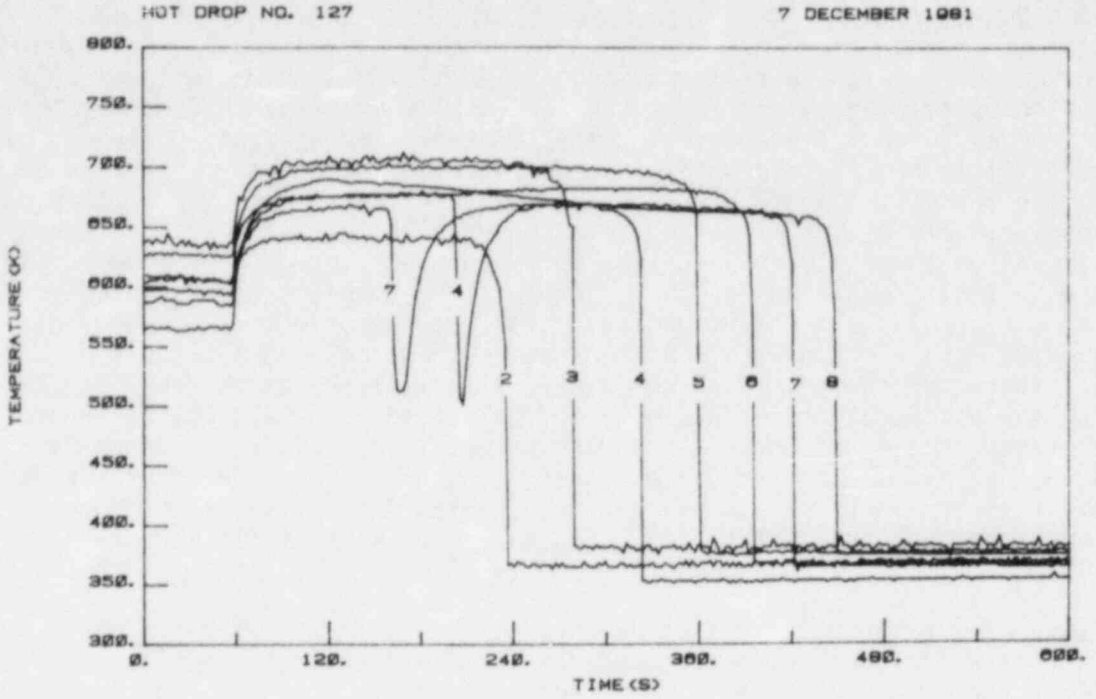

FIG. 4.8 Results of Run No. 127: Temperature Traces

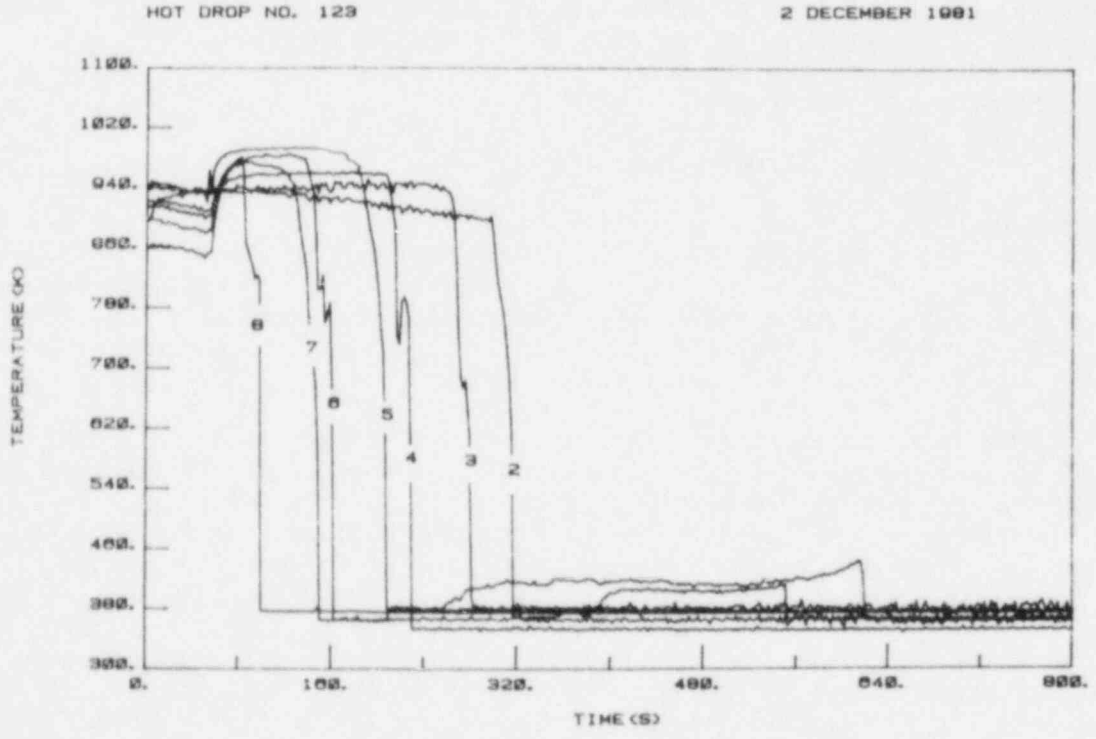

FIG. 4.9 Results of Run No. 123: Temperature Traces

cooling progression. The quench propagation results are discussed further in Section 4.6.2.

As discussed earlier in this section, Run No. 127 was an exceptional case in which a downward-progressing front was not clearly discernable from the temperature traces. Figure 4.8 shows the results of this experiment. Only two of the seven particle bed thermocouples showed an initial temperature drop associated with the arrival of a downward-directed cooling front. The temperature drops, however, were incomplete (i.e., the temperatures did not fall to the liquid saturation temperature). The two thermocouples subsequently reheated to nearly the initial temperature of the spheres. TC8 in this case responded very little to passage of the downward-moving front. At approximately 114 seconds (see Fig. 4.8), the slope of the TC8 temperature trace changed and the trace suggests a subsequent slow cooling behavior. A sharp temperature drop associated with liquid contact is absent. The arrival of the downward-moving front to TC8 is taken as 114 seconds. A downward-directed front is discernable in Fig. 4.9, but it is not as distinct as it is for most of the experimental runs. The upward-directed front is clearly defined in Fig. 4.8(b), which shows that the wall and the bed underwent a final quench process with little time lag between them.

Because of the "peculiarity" of Run No. 127, two additional experiments, Run Nos. 128 and 130, were performed under nominally identical conditions. The temperature traces, not shown here, are similar to those shown in Fig. 4.6 for Run No. 129. A clear pattern of a downward-directed front is observed in each case, followed by the upward-moving cooling front. All thermocouples in the particle bed responded sequentially from top (TC8) to bottom (TC2) in distinction to the result of Run No. 127. The frontal behavior of the results for the three runs is summarized in Fig. 4.10. The data show a consistent and reproducible pattern of bed cooling. The data of Run No. 127 are consistent with those of Run Nos. 128 and 130, even though not all of the thermocouples indicated passage of a cooling front.

4.5.2 Particle Bed Quench Propagation Data

Figures 4.10-4.13 present the particle bed quench-front propagation results for each of the four initial particle temperatures considered, with a fixed water temperature of 363 K. Each figure represents a composite (except for Fig. 4.13) of two or more experiments repeated under the same nominal conditions. The figures show the wall-cooling frontal progression as well as the upward- and downward-directed frontal progression.

The quench front data presented in Figs. 4.10-4.13 suggest a clear pattern of frontal cooling behavior for all the experimental conditions. A downward-moving front progresses to the bottom of the particle bed, at which time a front begins to propagate upwards. The test section wall and the particle bed usually quenched together in the upward quench progression when the initial wall temperature matched the initial bed temperature. When the wall temperature was initially larger than the bed temperature (Run No. 108), the wall quenched in a separate quench pattern. This is observed in Fig. 4.10, where the shaded square data points represent conditions in which the wall temperature was initially 672K, while the sphere temperature was initially 533K.

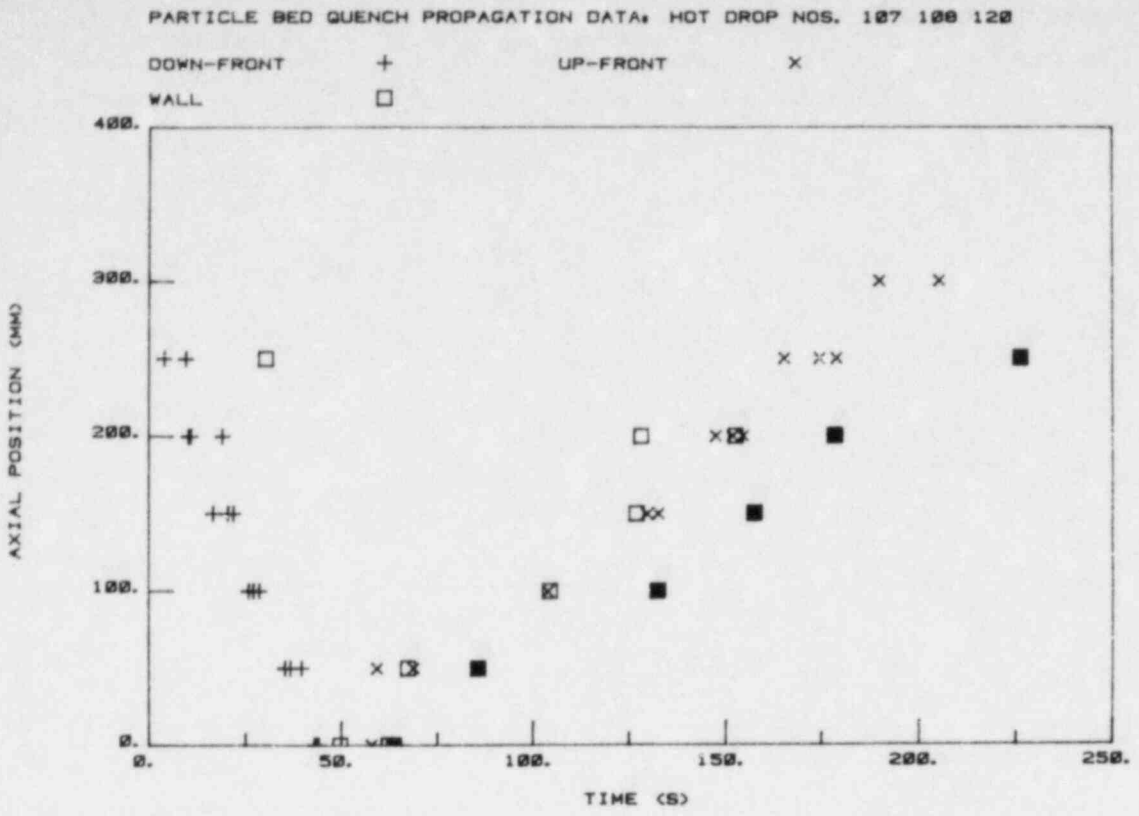

FIG. 4.10 Frontal Propagation Results: T_0 = 533 K

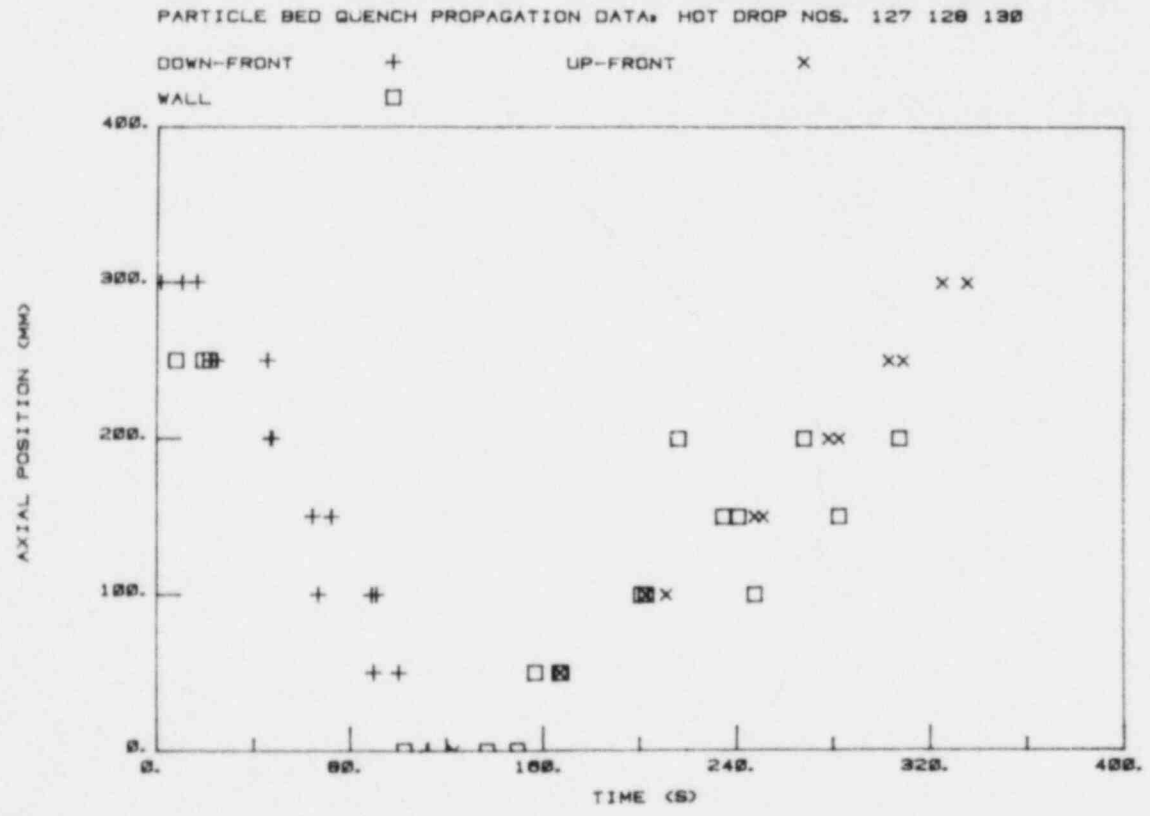

FIG. 4.11 Frontal Propagation Results: T_0 = 672 K

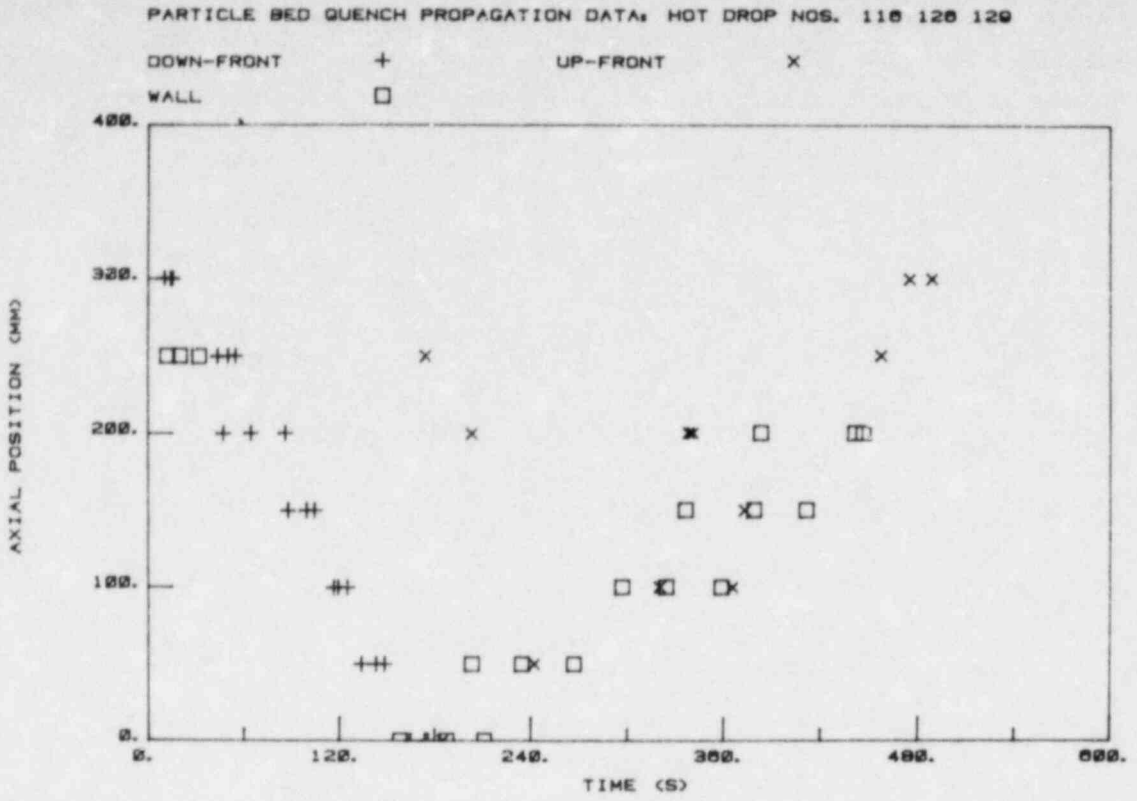

FIG. 4.12 Frontal Propagation Results: T_0 = 811 K

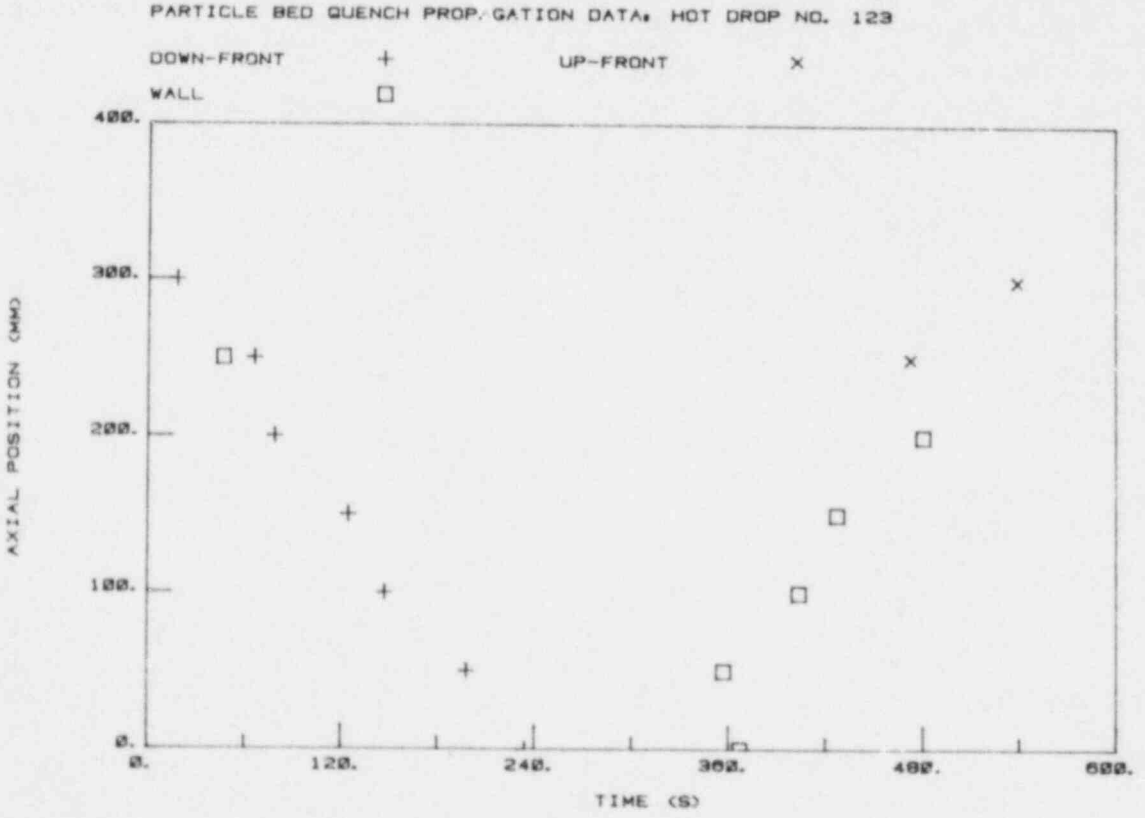

FIG. 4.13 Frontal Propagation Results: T_0 = 977 K

This delayed wall quench mode did not affect the prior downward- and upward-directed bed quench behavior.

Passage of the upward-directed cooling front past any axial location was coincident with the final quench of the thermocouple at that location. In no case is there any indication of subsequent thermocouple temperature rise after this front had passed.

In some of the individual experiments, especially at the higher sphere temperatures, only 2 or 3 thermocouples indicate passage of the upward-directed front. When plotted on the same figure, however, the superposition of several sets of data run under identical conditions reveals a clear pattern of frontal behavior.

4.6 Effect of Water Temperature

Experiments were performed with cooling water temperature in the range 274 K - 363 K (34 F - 190 F). Observation of the temperature traces suggest a trend whereby the lower the water temperature, the lower the likelihood of thermocouple temperature recovery following passage of the downward-directed cooling front. The temperature rise associated with recovery also tends to be smaller for the lower water temperatures.

In order to exaggerate the effect of water temperature, experiments were performed using ice water, at approximately 274 K. The most marked effect was observed with initial sphere temperature at 533 K. Of the four experiments listed in Table 4.1, which were run at 274 K under the same conditions, only one, Run No. 121, showed significant temperature recovery. The temperature traces for this run were similar to those of Run No. 107, presented in Fig. 4.7. The remaining three experiments, Run Nos. 118, 124 and 125, showed little or no temperature recovery. The temperature traces of Run No. 124 are shown in Fig. 4.14. Only TC3 shows signs of recovery. The remaining thermocouples stay at saturation temperature or show signs of incursions of cold water from the pool above the particle bed.

The other experiments listed in Table 4.1, which were conducted with water temperature less than 363 K, all show less temperature recovery following passage of the downward-directed front than the experiments with water temperature at 363 K.

4.7 Effect of Particle Bed Height

The effect of bed height was investigated in a series of three runs with initial sphere temperature 810 K and water temperature 363 K. The bed heights for Run Nos. 133, 116 and 132 were 200, 300 and 400 mm, respectively. The results of these experiments are summarized in Fig. 4.15, which show the frontal propagation data.

The data shown in Fig. 4.15 include the down-front and wall-cooling front information. The effect of bed height is simply to shift the time and position intercepts. The slopes of the frontal position vs. time lines are not appreciably influenced by the bed height. The magnitude of the frontal speeds is discussed further in Section 4.7.

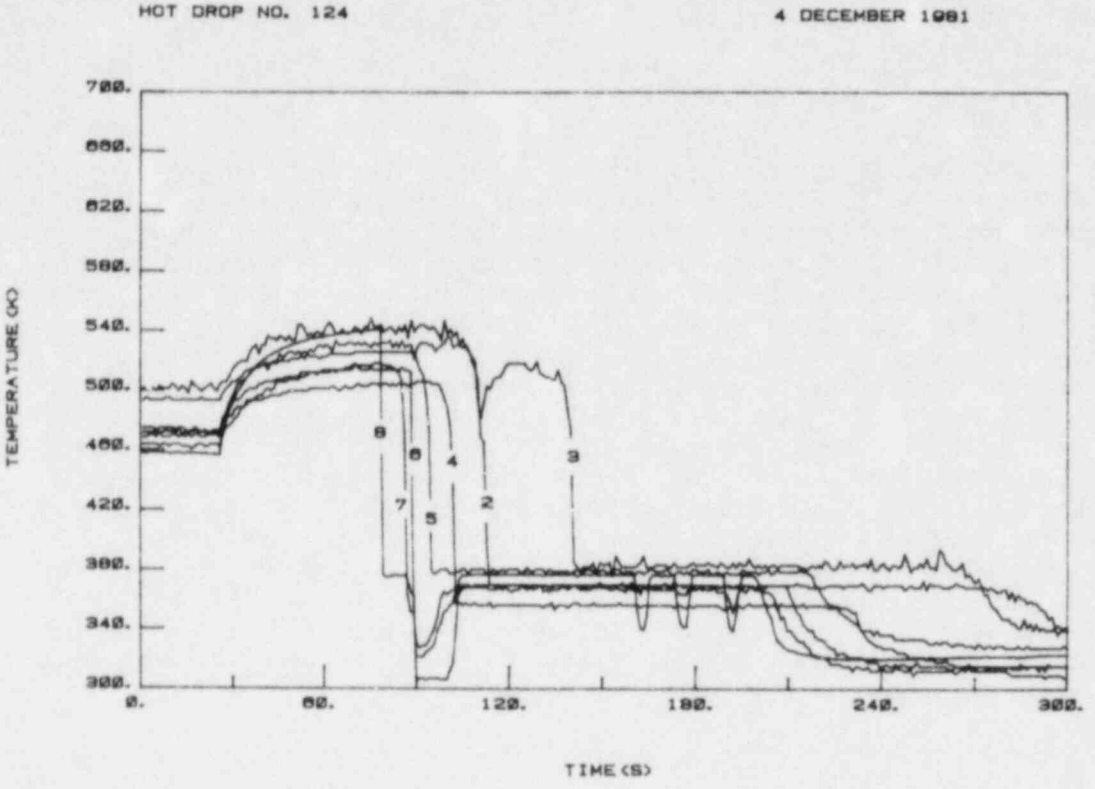

FIG. 4.14 Results of Run No. 124: Temperature Traces

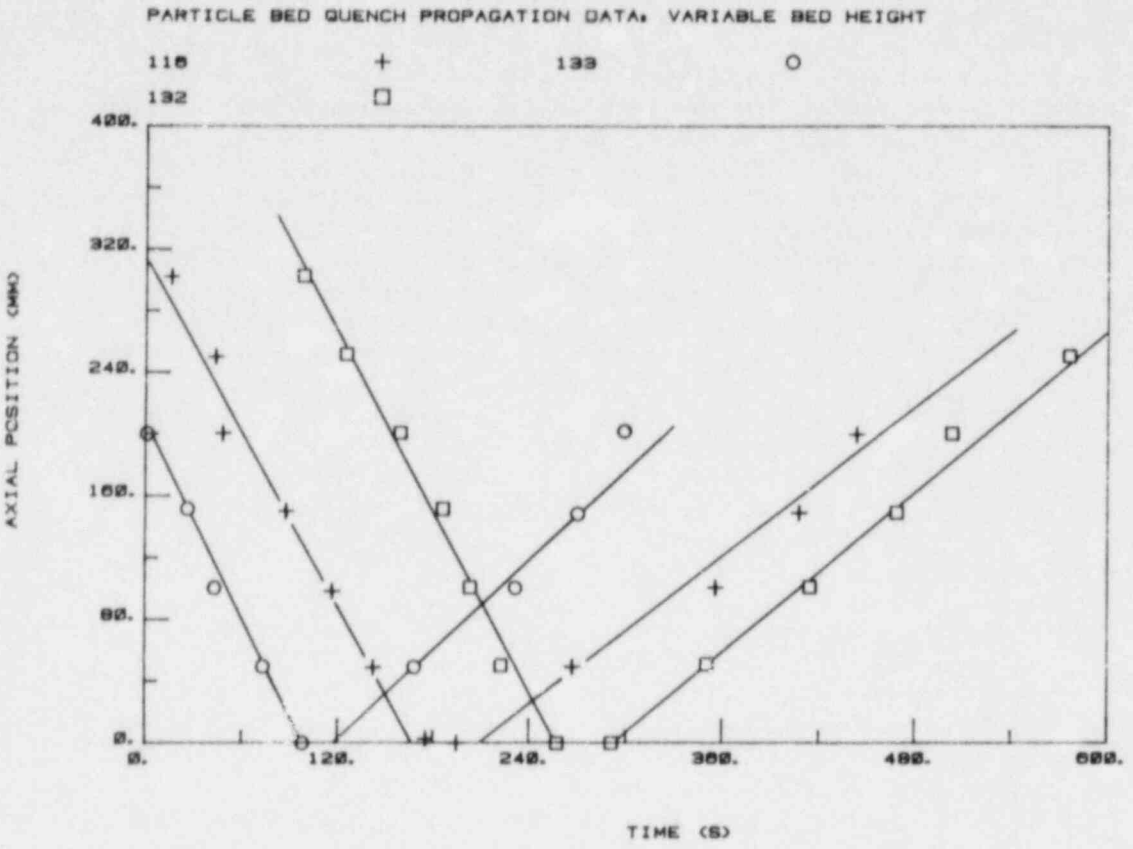

FIG. 4.15 Effect of Particle Bed Height on Frontal Propagation Results
Run 133, H = 200 mm; Run 116, H = 300 mm; Run 132, H = 400 mm

4.8 Particle Bed Quench Times

This section discusses various time scales useful for characterization of the quench characteristics of particle beds. The information is presented in tabular form in Table 4.2.

The "quench time", t_q, is defined as the time, measured from initial particle-water contact, required for the spheres to reach thermal equilibrium with the cooling water. At this time the particles will have been cooled to the liquid saturation temperature and boiling will have ceased. The time required for quenching of the particle beds was obtained (i) from observation of the pressure transducer (PT) signal, and (ii) from the temperature trace results. The pressure transducer provides an estimate of the time interval during which boiling occurred within the test vessel. The temperature traces give an indication of the time lapse between the first contact of liquid with the uppermost thermocouple and the final passage of the upward-directed cooling front past the thermocouples. Figure 4.16 compares the pressure transducer and thermocouple estimates of the bed quench time, PT-TIME and TC-TIME (t_q^{TC}). The pressure transducer estimate is consistently larger than the thermocouple-derived measurement of the overall quench time. It is believed that the reason for the larger values of the pressure transducer time scale (PT-TIME) are the result of continued boiling in the test section due to stored energy in the test vessel wall. It is felt that the thermocouple-derived quench times are more representative of activity within the bed than the transducer-derived times. Figure 4.17 presents the bed quench times plotted against the initial particle temperature difference. All runs are plotted except for Nos. 24 and 25. The bed quench time increases with temperature difference, or particle stored energy. These quench times are used in Section 4.10 to compute the average bed cooling rate.

Two additional time scales may be defined from the frontal propagation results: (i) the time, t_d, required for the downward-moving front to reach the bottom of the test vessel, and (ii) the time, t_u, for the upward-moving front to traverse the bed from top to bottom. The quantities, t_d, were obtained from the frontal propagation data, e.g., from Fig. 4.15. A linear least-squares analysis was performed on the down-front position vs. time data. The time t_d for the front to reach the bottom of the vessel is obtained from the least-squares fit equation. Since the downward-propagating frontal pattern was relatively easy to identify, evaluation of t_d for each experiment was straightforward. This time scale, furthermore, is reasonably reproducible. The time t_u, however, was somewhat more difficult to accurately specify. This quantity was obtained for each experiment by subtracting t_d from the overall quench time t_q^{TC}.

The quantities t_u and t_d extracted from the data are presented in Table 4.2. Figure 4.17 presents the frontal traverse times for all experiments with water temperature approximately 360 K. The results presented in Fig. 4.17 are used in particle bed heat transfer calculations presented in Section 4.10.

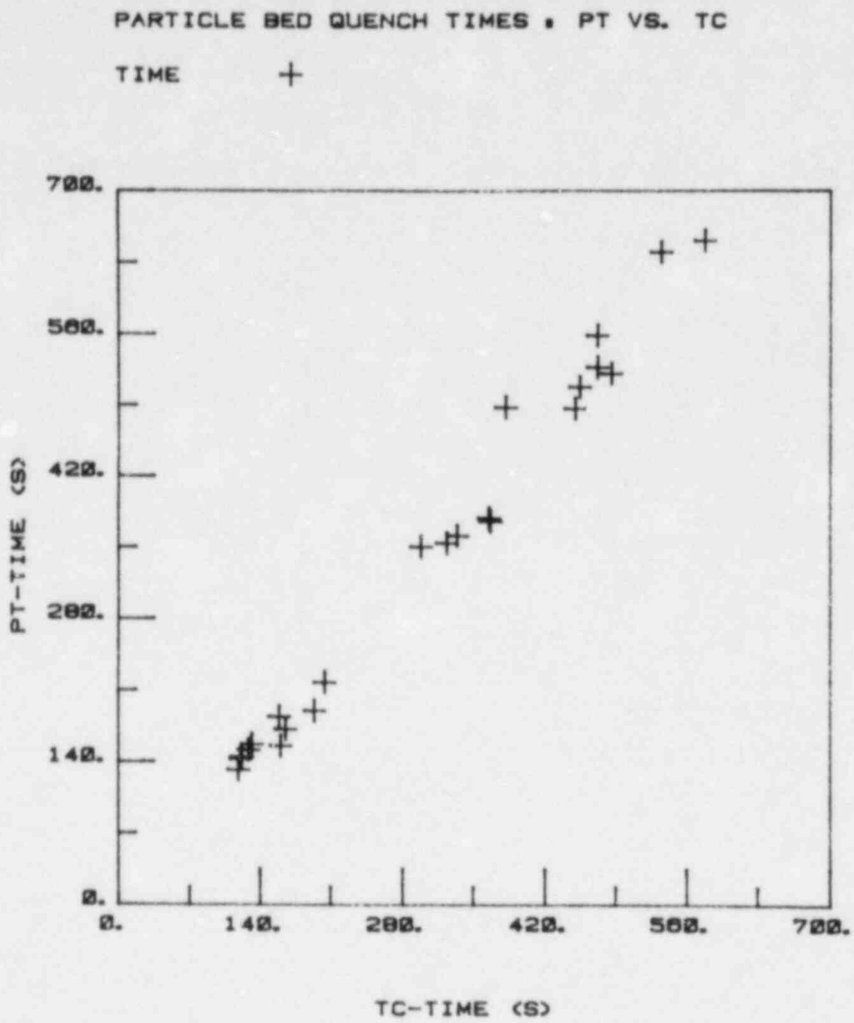

FIG. 4.16 Comparison and Pressure Transducer and Thermocouple Derived Bed Quench Times

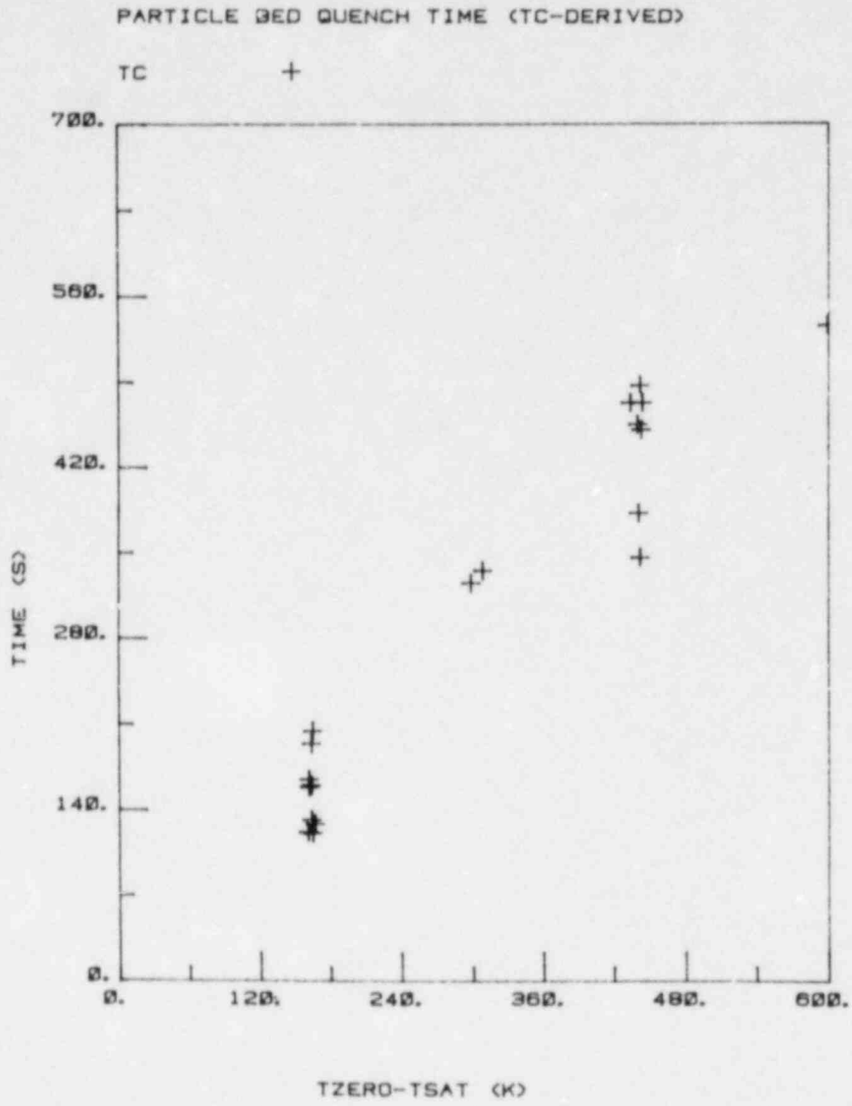

FIG. 4.17 Particle Bed Quench Time vs. Initial Particle Temperature Difference

4.9 Cooling Front Propagation Speeds

The temperature traces for each of the experiments were analyzed and a frontal propagation plot was constructed, as described in prior sections. In nearly all cases a clearly identifiable pattern of a downward-moving front was observed. The position vs. time data associated with the frontal pattern appeared linear. As a result of this observation a linear least-squares fit was performed for each set of down-front data and the speed of the front, v_d, was thereby obtained. Each experiment provided a well-defined v_d.

The frontal propagation plots also suggest the existence of an upward-propagating cooling front. This front, however, must be identified by a combination of wall and particle bed position-time data. Observation of the bed thermocouples alone in many cases does not suggest the existence of a frontal cooling pattern. The speed of the upward-directed cooling front, v_u, was obtained for each experiment in which three or more bed thermocouples appeared to suggest cooling front behavior.

The computed values of cooling propagation speeds are tabulated in Table 4.2. A v_d is presented for each experiment. For the reasons described above, however, it was not possible in many cases to compute a value of v_u. In most of the low initial sphere temperature experiments it was possible to compute a v_u. Most of the cases where a value of v_u could not be calculated occurred for high sphere temperature. This observation is consistent with the experimental results described in Section 2.5.

The frontal propagation speeds for all experiments are presented in Fig. 4.18. The results indicate that:

(i) the downward frontal speeds are 2-3 times greater than the upward speeds;

(ii) the frontal speeds fall off with initial stored sphere energy (proportional to $T_{ZERO}-T_{SAT}$);

(iii) the frontal speeds are more reproducible at the higher sphere temperatures;

(iv) the speeds are independent of cooling water temperature.

4.10 Particle Bed Heat Transfer Rates

The major objective of this study is to develop models for prediction of the steam generation rate resulting from the thermal interaction between cooling water and hot core debris.

In this section, the rate of heat transfer between the particle beds and water is estimated from the data presented in previous sections. Thus, while the particle-water heat transfer rate was not directly measured in this study, various estimates of the characteristic heat transfer rates are presented below.

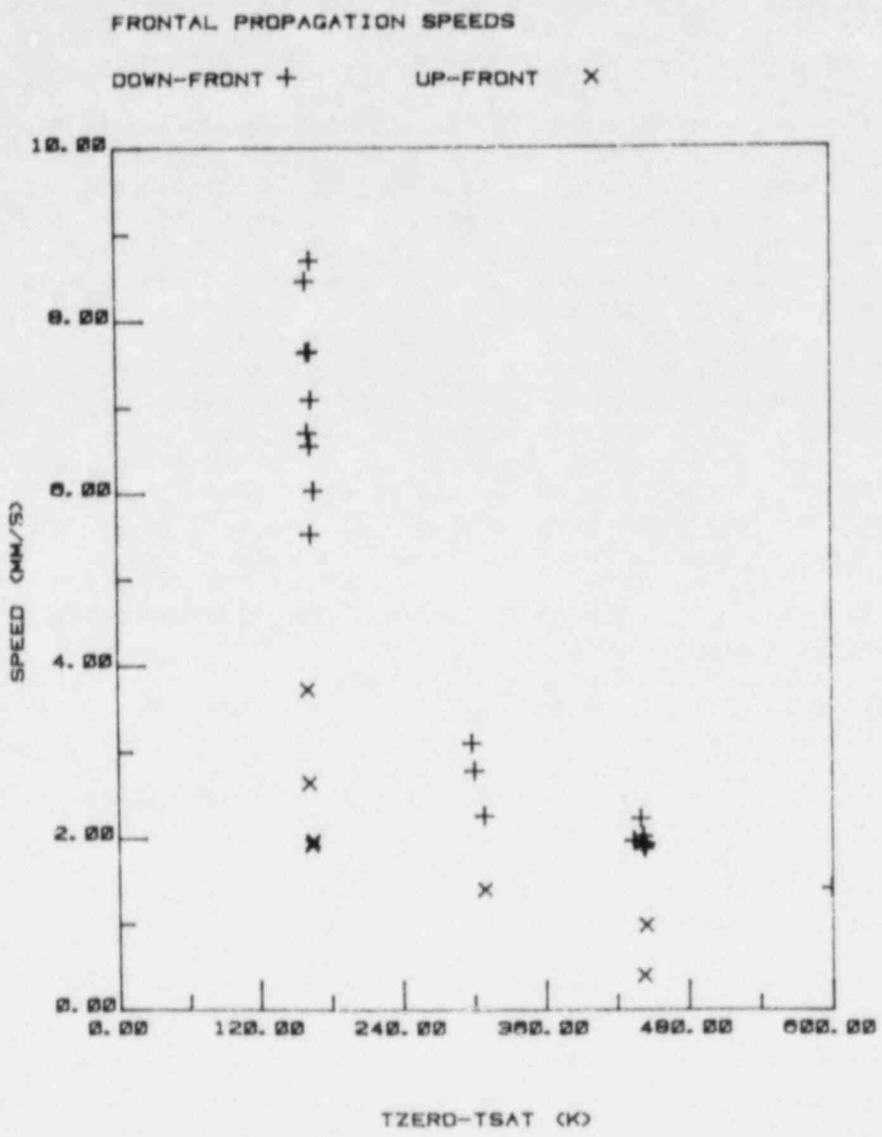

FIG. 4.18 Summary of Frontal Propagation Speeds

4.10.1 Average Bed Heat Flux

The average rate of heat transfer is defined by assuming that the initial stored energy of the spheres is transferred to the water in a time equal to the particle quench time, t_q. The heat flux based upon the test vessel cross-sectional area is, then

$$q''_{avg} = \frac{MC(T_o - T_{SAT})}{A\, t_q^{TC}} \tag{4.1}$$

Average heat fluxes were computed for each of the experiments using the quench times tabulated in Table 4.2. The resulting heat fluxes are presented in Table 4.2 and are also shown in Fig. 4.19.

The average heat flux data presented in Fig. 4.19 are, within experimental scatter, independent of the initial particle bed temperature difference $T_o - T_{SAT}$ (or stored energy). This observation suggests that the particle bed heat transfer rate is independent of temperature driving potential. The data also suggest that the ice water experiments led to higher heat transfer rates than those conducted at higher temperatures.

4.10.2 Maximum Bed Heat Flux

The cooling front propagation data discussed in prior sections suggest that bed cooling occurs in two stages, corresponding to the time periods of the downward- and upward-propagating cooling fronts. It is likely that the heat transfer rates during the two time periods differ from each other and from the average heat transfer rates defined in Section 4.9. Since the instantaneous heat transfer rate was not measured in this experiment, it is not possible to directly evaluate the heat fluxes during the two time periods. An upper limit estimate of the heat transfer rate during bed quenching can be obtained by assuming that all of the heat transfer occurred during the time of passage, t_d, of the downward cooling front. The maximum heat flux can then be computed as

$$q''_{max} = \frac{MC(T_o - T_{SAT})}{A\, t_d} \tag{4.2}$$

A value of q''_{max} was computed for each experimental run, using the values of t_{down} listed in Table 4.2. The resulting q''_{max} are listed in Table 4.2 and are shown in Fig. 4.20. Except for the lowest sphere temperature data, the results also suggest that the bed cooling rate is independent of the driving temperature difference. There is some evidence of a water temperature effect, as observed in Section 4.10.1. Data scatter, however, precludes a clear conclusion.

4.10.3 Summary of Computed Heat Transfer Estimates

The heat transfer information presented in Sections 4.10.1 and 4.10.2 are calculational estimates based upon several quantities which were measured.

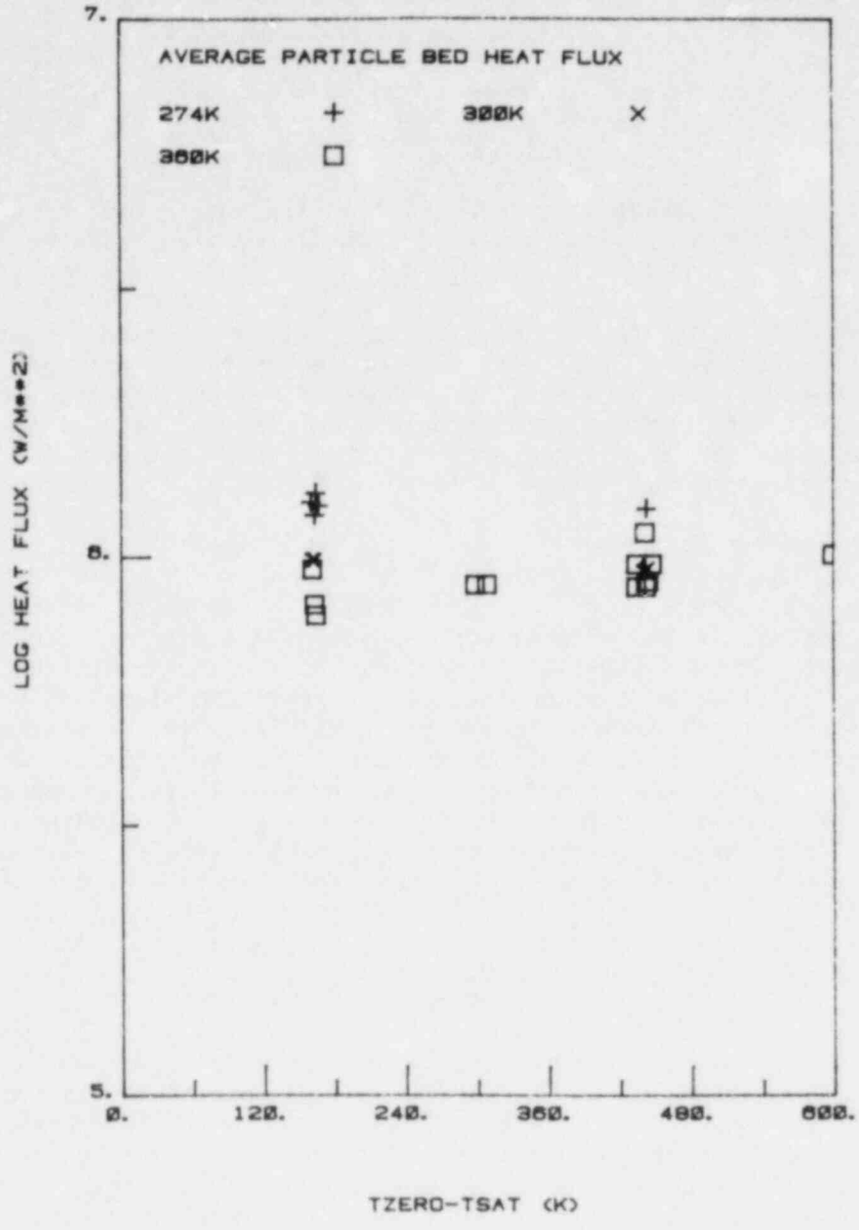

FIG. 4.19 Estimate of Average Particle Bed Heat Flux

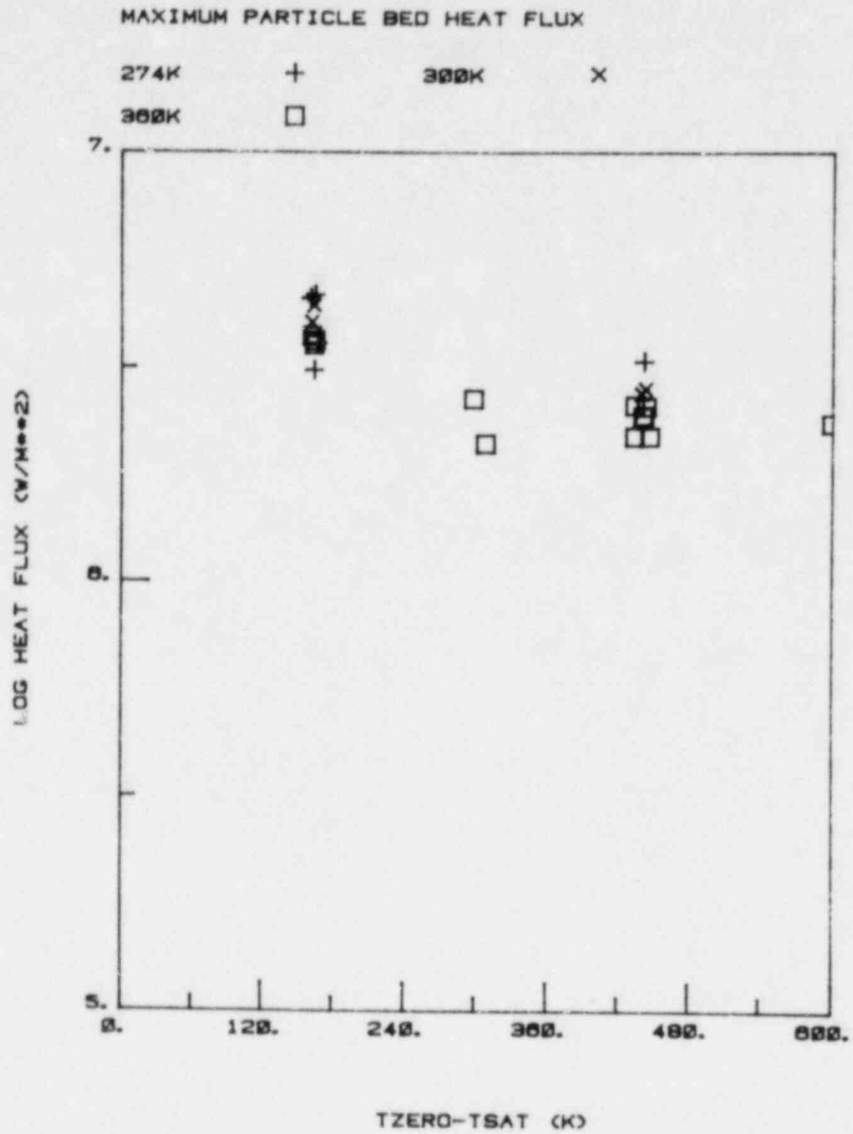

FIG. 4.20 Estimate of Maximum Particle Bed Heat Flux

Particle bed heat transfer rates were not directly measured. This section summarizes the computed heat transfer estimates.

The calculated average and maximum heat fluxes are compared in Fig. 4.21. They indicate that the particle bed heat flux is in the range 1.0×10^6 to 2.5×10^6 W/m^2 for the conditions of the experiments. Except for the experiments with the lowest sphere temperatures, the estimated particle bed heat removal rate is independent of sphere temperature.

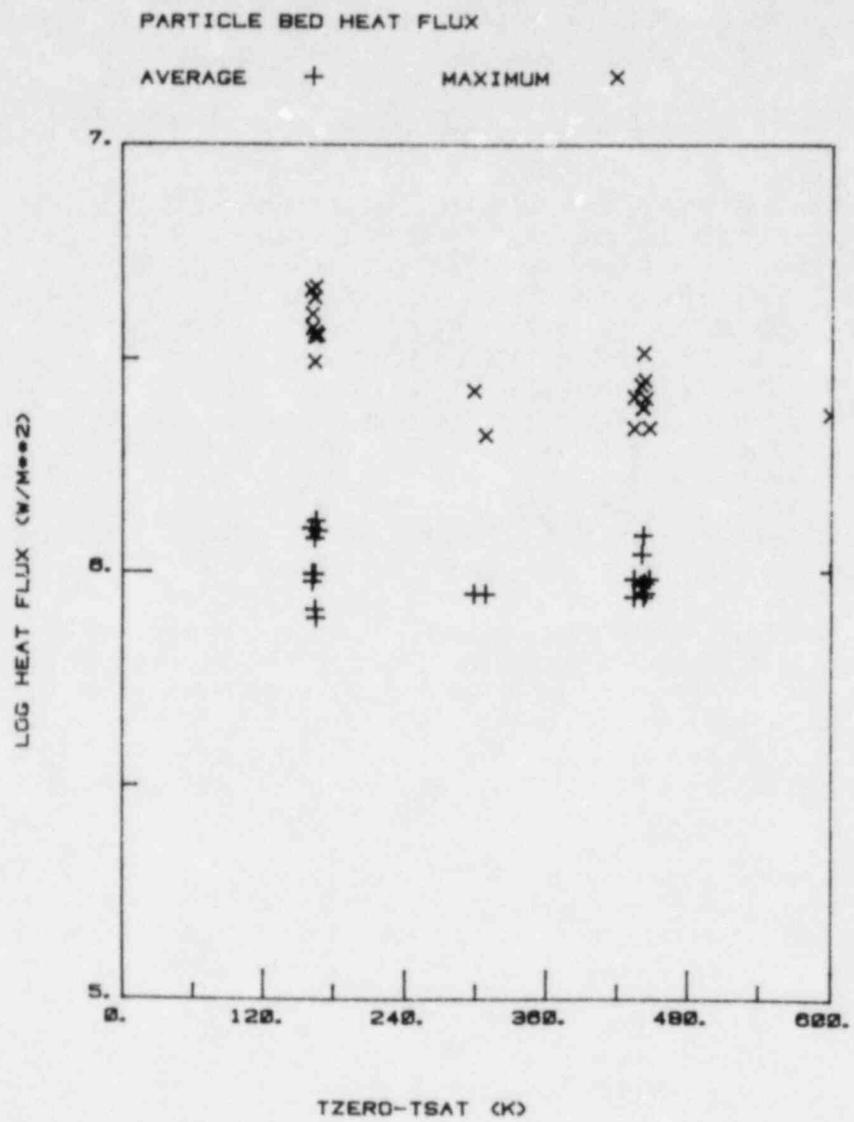

FIG. 4.21 Comparison of the Average and Maximum Experimental Particle Bed Heat Fluxes

5. DISCUSSION AND INTERPRETATION OF RESULTS

This chapter synthesizes the experimental observations presented in Chapter 4 into a picture of the particle bed quenching process. Section 5.1 presents an interpretation of the experimental results. A mathematical model for the physical processes involved in particle bed quenching is discussed in Section 5.2.

5.1 Heat Transfer Characteristics of Superheated Particle Beds Under Transient Quench Conditions

The experimental evidence presented in Chapter 4 suggests that two cooling frontal patterns propagate sequentially through a superheated bed when flooded from above with water. A downward-propagating cooling front begins to traverse the particle bed immediately upon introduction of cooling water. This frontal behavior is characterized schematically in Fig. 5.1(a). The cooling front, located at z^*, is postulated to separate an upper region into which water has penetrated and in which the spherical particles are partially quenched, from a lower region into which water has not yet penetrated. The advance of the cooling front is observed experimentally by the initial pattern of thermocouple temperature drops, described in Chapter 4 and characteristic of nearly all of the experiments. The upper layer is not completely quenched, i.e., not all of the particles are reduced to the water saturation temperature, as indicated by the thermocouple "recovery" observed in many of the experiments. This downward-propagating front is postulated to be associated with the first arrival of liquid to the thermocouple locations. Prior to arrival of the front, the particles are dry. The downward-propagating cooling front advances with speed v_d. The speed v_d is a decreasing function of the initial stored energy, as shown in Fig. 4.18. The downward-moving front reaches the lower boundary of the test vessel at time t_d following initial contact of the water with the bed. This time increases with bed height and initial stored sphere energy, as shown in Fig. 4.17.

The experimental evidence suggests that upon arrival of the downward-directed front to the lower boundary of the particle bed the particles were incompletely quenched. This is clear from observation of the thermocouple traces from most of the experimental runs. Exceptions to this behavior occurred for runs with water temperature near the ice point. In some of these cases quenching of the particle bed, as indicated by the bed thermocouples, was complete upon passage of the initial water front. It is noted, however, that some 294 K water runs exhibited only partial quenching.

A direct evaluation of the energy removed during passage of the downward-propagating front is not possible from the data of this experiment. The temperature and liquid-fraction distributions within the bed at any instant are not known. The thermocouples are used only to provide an indication of the presence or absence of water at the site of the thermocouples. A thermocouple reading above T_{SAT} was used to infer that the spheres surrounding the thermocouple were above the liquid saturation temperature. The actual sphere temperatures were not inferred from the thermocouple traces. As a consequence, the

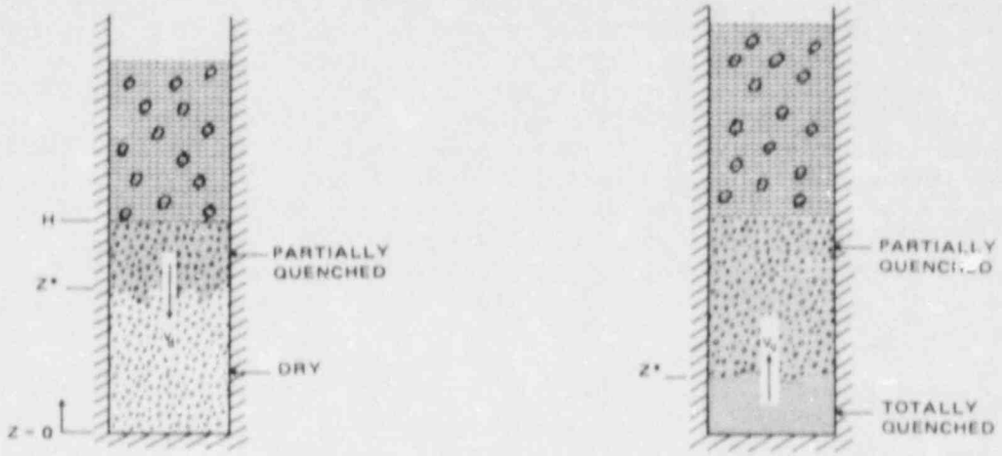

(a) (b)

FIG. 5.1 Illustration of Frontal Progressions

(a) Downward (b) Upward

total energy removed from the spheres during passage of the downward cooling front cannot be directly obtained from the bed thermocouples. All that is known directly from the data is that some fraction of the initial stored energy was retained in the spheres after passage of the downward cooling front. It is postulated that there existed pockets or channels of spheres which were left unquenched subsequent to passage of the downward-progressing coolant front.

A second cooling front is postulated to develop upon arrival of the initial front to the bottom of the test column. This frontal pattern propagates in the upward direction, as shown schematically in Fig. 5.1(b), at a speed v_u. The existence of this front is suggested by the observed sequences of final bed thermocouple temperature drops in many of the temperature traces. This pattern of sequential temperature drops is most apparent in the experiments performed with 533 K initial sphere temperature and with 360 K water. In these experiments nearly all thermocouples show temperature rises following passage of the downward cooling front. These thermocouples are finally reduced to the saturation temperature in a sequential pattern from bottom to top of the test vessel. The thermocouples subsequently exhibit no departure from the liquid saturation temperature. At the higher sphere temperatures, and with 360 K water, this behavior becomes less pronounced. Only a fraction of the bed thermocouples exhibit temperature rises following passage of the downward front. In general, these thermocouples then show a final temperature drop in a sequential pattern which suggests the passage of an upward cooling front. The pattern, however, is not as clear as for the 533 K sphere temperature experiments.

The wall thermocouple traces support the hypothesis of the passage of an upward-directed cooling front. In the experiments with heated test wall, the wall temperatures remained close to the initial temperature during passsage of the downward cooling front. The final, rapid temperature drop of these thermocouples, associated with the transition from film-to-nucleate-boiling, occurs in a sequential pattern from bottom to top of the test vessel. With the wall temperature preheated to the sphere temperature, the final quench of the bed thermocouples coincides in time with that of the wall thermocouples. With the wall heated above the sphere temperature, the wall quenches later than the corresponding bed thermocouples.

The combination of particle bed and wall thermocouple temperature traces suggests that a second cooling front propagates up the column subsequent to arrival of the downward-moving front to the bottom of the vessel. It is hypothesized that the final quench of the particle bed occurs during passage of this cooling front up the test column. That is, it is postulated that the passage of the upward-propagating quench front, indicated by final quench of the thermocouples within the packed bed, coincided with the final quench of the spherical particles as well. If the spheres had retained significant internal energy after passage of the upward-directed cooling front, it is argued that the thermocouples would have dried out and would have indicated the presence of superheated spheres, as they did following passage of the downward-directed front. This hypothesis will be further evaluated in future experiments.

The upward-propagation front is assumed to move at speed v_u and to take t_u seconds to traverse the particle bed. The propagation velocity is a

decreasing function of $T_o - T_{SAT}$. The speed of the upward-propagating front, derived from the particle bed thermocouples, is approximately half that of the downward-directed front.

The heat transfer rate between the particle bed and cooling water was not directly measured in the experiments. Estimates of the heat transfer rate, however, were made using the time scales t_u and t_d, together with the initial stored energy. The average particle bed heat flux, defined by Eq. (4.1), was shown to be independent of particle temperature difference, $T_o - T_{SAT}$, as shown in Fig. 4.24. The magnitude of the observed heat flux is 10^6 W/m^2. The particle bed cooling rate, then, is independent of the driving temperature difference for particle-water heat transfer, for ΔT up to 600K.

5.2 Transient Particle Bed Heat Transfer Mechanisms

The experimental results reported here are used to provide insights into the limiting particle bed heat transfer mechanisms operative during the transient bed cooling process. The discussion presented here is preliminary, however, since the range of parameters studied thus far is limited, and a direct measurement of the particle bed-water heat transfer rate has not yet been made.

Insight into possible heat transfer mechanisms can be gained by comparison of single-particle heat transfer time scales to the measured particle bed quench time scales. Assume that the particle bed has been completely submerged in water, such that *each* particle is surrounded by water. The particles are assumed to transfer heat to the surrounding water through a film-boiling heat transfer process. A lumped-parameter heat transfer equation for a particle in film boiling is

$$m_p c \frac{dT}{dt} = h_{fb} A_p (T - T_{SAT}) \qquad (5.1)$$

where it is assumed that the water is at the saturation temperature and that the internal resistance to heat transfer is negligible. The time constant for a sphere is

$$\tau_p = \frac{m_p c}{h_{fb} A_p} = \frac{\rho c d}{6\, h_{fb}} \qquad (5.2)$$

Using the Bromley (1950) film boiling heat transfer correlation, the heat transfer coefficient for a 3 mm sphere is approximately constant at 350 W/m^{2}K for temperatures up to 1300 K at atmospheric pressure. The time constant, then, for a 3 mm stainless steel sphere is 6-7 seconds. This time scale is interpreted to be the order-of-magnitude of time which would be required to quench the particle bed if water were available to all the particles in the bed immediately upon introduction of cooling water.

The particle bed quench times measured in the experiments were in the range 120 to 600 seconds for initial particle temperatures in the range 533 K to 971 K, as shown in Table 4.2.

The large disparity in the computed particle film-boiling time scale and the measured bed quench times suggests that the controlling rate process is not related to individual particle-water heat transfer resistance.

The computed average heat flux results presented in Fig. 4.19 indicate that the particle heat removal rate is independent of T_o-T_{SAT}, the driving temperature differential for particle-water heat transfer. This observation provides further evidence that particle-water film boiling heat transfer is not the mechanism which controls the particle bed cooling rate.

The frontal characteristics of the experimental data suggest that the particle bed heat transfer rate is limited by the rate of supply of water to the dry, yet unquenched, regions of the bed. A process which would limit the flow of water to the dry regions of particle beds during transient heat removal is countercurrent two-phase flow flooding. The flooding phenomenon is suggested by prior work involving maximum steady-state heat removal from internally heated particle beds, discussed in Section 2.4.

The heat removal rates predicted by steady-state debris bed maximum heat transfer models are presented in Fig. 5.2 for the packed particle bed conditions of the experiments reported here. Figure 5.2 also presents the steady-state experimental data of Barleon (1981) for 100 mm-depth particle beds with particle sizes greater than 1 mm. The transient quench data from the present experiment are presented in Fig. 5.2 as a black band. The band represents a range of heat transfer rates bounded by $q"_{max}$ and $q"_{avg}$, which were established from the experimental data. This range of estimates arises, rather than a simple quantity, because of the uncertainty in the fractions of particle stored energy transferred to water during the two frontal propagation periods. (This uncertainty will be resolved in future work.) Figure 5.2 indicates that the average heat flux $q"_{avg}$ agrees reasonably well with the models of Lipinski (1980) and Gabor (1980). It also agrees well with the steady-state data of Barleon (1981). The "d^2"-dependence of the heat flux characteristics of the laminar regime model of Gabor, however, does not well-characterize the Barleon data. The best agreement with the available data, both steady-state and transient, in magnitude and trend is provided by the counterflow turbulent regime model of Lipinski. This model predicts a "$d^{1/2}$"-dependence of the heat flux on particle diameter.

The steady-state models are all countercurrent two-phase flow packed bed flooding criteria. The mechanism which governs the maximum heat removal rate is a hydrodynamic limitation which governs the supply of liquid to the bed from the overlying pool. It is plausible, although sufficient data have not yet been developed to make a conclusive case, that similar flooding criteria apply to the transient particle bed cooling process. Based upon the experiments reported here, the average particle bed heat removal rate under transient quench conditions encountered in the experiments are predicted using the steady-state model of Lipinski. Additional experimental data are required in order to allow a more definitive conclusion.

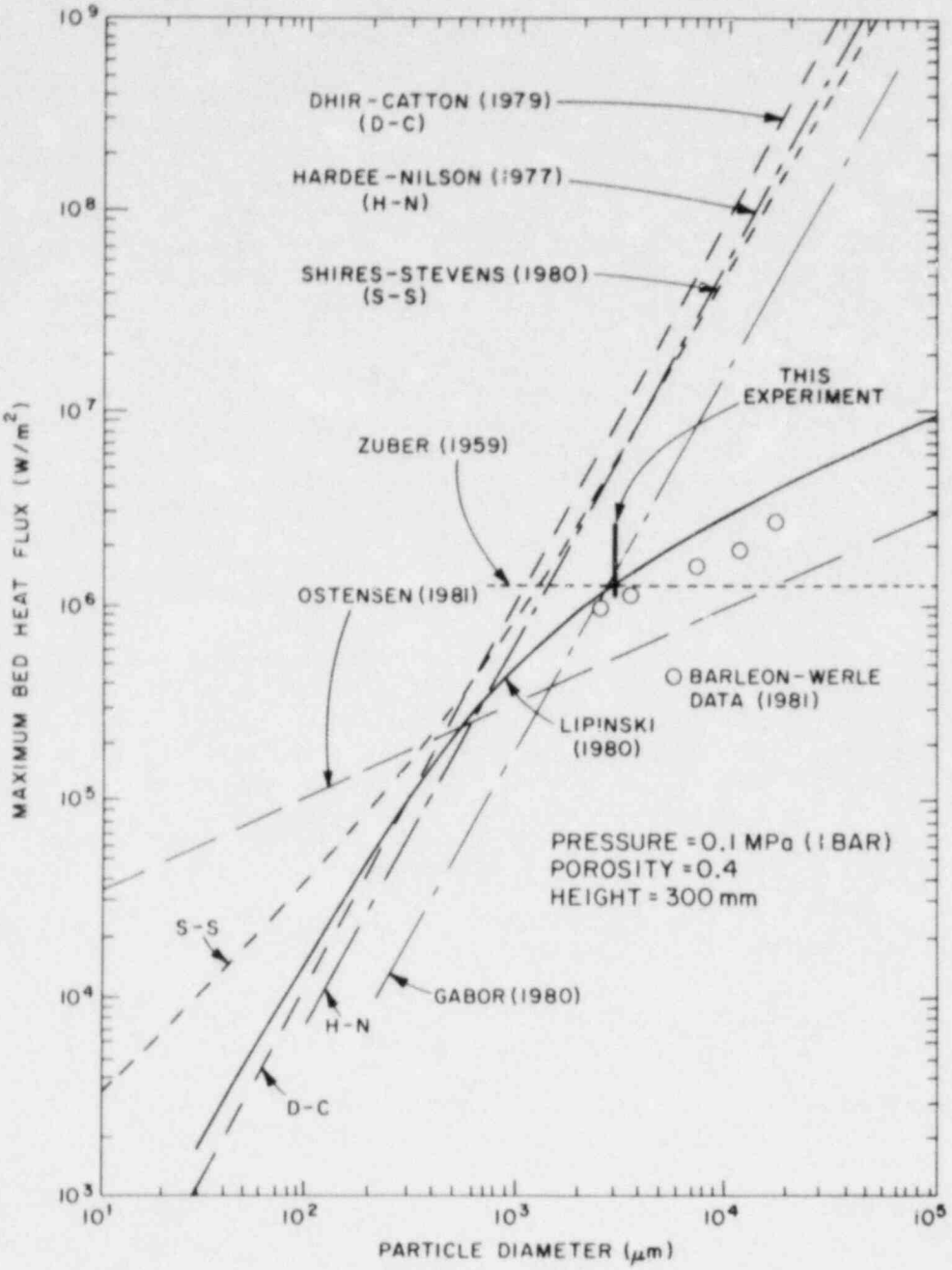

FIG. 5.2 Comparison of Bed Heat Transfer Models with Experimental Data

6. IMPLICATIONS WITH RESPECT TO LWR DEGRADED CORE ACCIDENTS

6.1 Accident Analysis Implications

6.1.1 LWR Steam Spike Containment Pressurization

Meyer (1981) has argued that the rate of containment pressurization as a result of core-debris-water-thermal interaction in TMLB' accident sequences can be conservatively bounded using the MARCH code's HOTDROP single-particle heat transfer model. Yang (1981) and Corradini (1981) substantiated this argument by arguing that the core debris would settle into a packed bed in the reactor cavity. They showed that if the transient heat removal rate from the bed is computed on the basis of steady-state debris bed heat transfer models, then the containment pressurization rate due to steam generation would be substantially lower than predicted by HOTDROP.

As discussed in Chapter 2, the thermal interaction between core debris would occur in several stages, two of which are the particle fall period and the packed bed period. MARCH treats the entire interaction using the HOTDROP model. Data have been obtained in this experiment for the packed bed period. The data obtained from the experiment support the above arguments, albeit for a restrictive set of experimental conditions.

Table 6.1 summarizes the various estimates of the experimental particle bed heat transfer rates. The quantity q''_{fb} in Table 6.1 is an estimate of the heat flux based on assumptions which are directly analogous to those of the HOTDROP heat transfer calculation. The Bromley (1950) film boiling heat transfer model for spherical particles is used to compute the total rate of heat transfer, assuming all particles are surrounded by water and participate in the interaction. Thus, the total particle surface area is used in the calculation. The heat flux q''_{fb} is then expressed in terms of unit bed cross-sectional area, as are the other heat fluxes in Table 6.1. The heat fluxes computed from various steady-state debris bed models are compared with those of the (transient) experiments.

The following conclusions are drawn from the comparison:

(i) The single-particle film boiling model, with assumptions analogous to HOTDROP, provides an overestimate of the experimentally determined transient particle bed heat removal rate. The film-boiling heat flux is an order-of-magnitude greater than any of the experimental heat fluxes.

(ii) Estimates of the average transient packed bed heat removal rates determined experimentally are predicted reasonably well by the steady-state countercurrent-flow limited heat transfer models. The quantity q''_{max}, an upper-bound estimate of the experimental heat flux, is, however, approximately a factor of two above the predictions.

TABLE 6.1

Particle Bed Heat Removal Rates

Particle Diameter	3 mm
Porosity	0.4
Bed Height	200-400 mm
Pressure	0.1 MPa (1 Bar)

This Transient Experiment (W/m^2)	Steady-State Debris Bed Model (W/m^2)		Sphere Film Boiling ΔT = 165 K, 15 kg Steel (W/m^2)
$q''_{avg} = 1.0 \times 10^6$	Shires	8.0×10^6	$q''_{fb} = 2.6 \times 10^7$
$q''_{max} = 2.5 \times 10^6$	Hardee	7.9×10^6	
	Dhir	1.3×10^7	
	Theofanus	1.3×10^6	
	Lipinski	1.3×10^6	
	Zuber	1.1×10^6	
	Gabor	1.5×10^6	
	Ostensen	5.5×10^5	

Thus, the data support the contention that the HOTDROP model assumptions provide an overestimate of the heat transfer during the packed bed period of the thermal interaction. Data for the particle fall period are required in order to generalize the conclusion to the entire thermal interaction process, including both fall and bed periods.

The conclusions discussed above are based upon the data presented in this report, the conditions of which do not encompass those of prototypic interest. Further data and model development are required in order to more confidently extrapolate the conclusions to prototypic conditions.

6.1.2 Transient Debris Bed Heat Removal: Basic Model Assumptions

Calculation of the core debris-water thermal interaction using either the HOTDROP model or debris bed models implicitly assume that if the debris are fragmented, then they are coolable in the sense that their stored energy can be successfully removed while in a debris bed configuration. Based upon the assumption of coolability, it is then further assumed that the debris bed cannot attack the reactor cavity basemat. This set of assumptions rules out the possibility of concrete decomposition and gas release during the time period of transient heat removal from the debris bed. It also implies that bed heat removal is not influenced by concrete decomposition gases. The results of the experiments reported here suggest that these assumptions and implications may be invalid.

The discussion in Section 5.1 of transient cooling of packed beds suggests that debris bed cooling occurs as a frontal process. Debris bed cooling would begin at the top of the bed and would proceed downward in a frontal pattern. Debris at any axial location would be devoid of cooling water until the downward propagating front reaches that location, and would therefore remain at its initial temperature until that time. Heat transfer from the debris bed to the concrete would occur until water penetrates to the bottom of the bed and reaches the concrete.

Consider a packed bed of core debris of uniform height which is initially at the steel melting temperature, whose characteristics are shown in Table 6.2. Cooling water must remove both decay heat and sensible heat from the debris. A model is being developed to account for both effects. A lower bound on the time period t_d for water to penetrate to the base of a superheated debris bed can be obtained by neglecting the effect of decay heating. Assume that the heat removal rate during the entire quench period is q''_{avg}. During the downward frontal period the frontal propagation speed v_d can be computed from the energy balance equation

$$q''_{avg} = f_d \rho c (1-\varepsilon) (T_o - T_{SAT}) v_d \qquad (6.1)$$

The quantity f_d is the fraction of initial sphere internal energy which is removed during the downward front period. Since the heat removal rate is assumed constant throughout the quench period, f_d can be computed from the times t_d and t_u as

$$f_d = \frac{t_d}{t_d + t_u} \qquad (6.2)$$

TABLE 6.2

Representative Debris Bed Characteristics*

Bed Depth	0.94 m (3.1 ft)
Porosity	0.4
Particle Size	3 mm
Initial Temperature (T_{ZERO})	1723 K
Containment Pressure	0.5 MPa (5 bars)
Water Saturation Temperature	425 K
$T_o - T_{SAT}$	1298 K
Heat Removal Rate**	2.4×10^6 W/m^2
Specific Heat	600 J/kg K
Density	8000 kg/m^3

*Conditions characteristic of Indian Point reactors (Meyer, 1981). Debris includes all steel. Bed covers entire reactor cavity area.

**Computed using the Lipinski model.

The data from Table 4.2 indicate, for the experiments with sphere temperature greater than 535K, f_d is approximately 0.35 to 0.40. That is, based upon the above assumptions, 35 to 40 percent of the initial particle internal energy is removed during the passage of the downward-propagating front.

For the conditions of Table 6.2, the speed v_d is computed as 1.61 mm/s. With a bed height of 0.94 m, the minimum time for the front to reach the cavity floor would be t_d = 589 seconds. For the time period t_d, the concrete would be heated by the debris above it, and the dry debris would reheat by decay heating. Remelting of at least the metallic component of the debris, therefore, must be considered.

The above calculation assumes that no gases are released from the concrete. During the time period t_d, however, the concrete would be attacked by the particulated core debris, and gases would be released. If the resulting gas flux is "sufficiently large", the gas may further limit bed heat removal by the countercurrent two-phase flow mechanism.

The implications of the above discussion are that:

(i) core-concrete interactions would begin simultaneously with bed formation, even though water is available for cooling;

(ii) it may not be possible to remove the stored energy from the fragmented core debris without remelting the debris, even if water is available.

At this point it is not known whether the core-concrete interactions described above would preclude eventual successful cooling of the core debris without prior remelting.

It should be noted that Meyer (1981) has computed the containment pressurization under assumptions which consider the above implications. He has assumed that the debris is not coolable and immediately interacts with the concrete, producing combustible gases. This calculation, using the MARCH code, "bypasses" the HOTDROP model. Steam is not produced and this leads to what is felt to be a lower-bound estimate of the containment pressure load.

6.2 MARCH Code Modifications Recommended

The experimental data and their interpretation suggest that modifications to the MARCH code are required to provide a more accurate description of the interaction between core debris and water following failure of the reactor vessel. The following issues should be addressed:

(i) The HOTDROP single-particle model should be coupled to a transient debris bed quenching model in order to allow calculation of the thermal interaction time periods discussed in Chapter 2.

(ii) A transient debris bed cooling model should be incorporated in MARCH to allow for tracking of the frontal propagation observed in the experiments.

(iii) The transient debris bed should allow for simultaneous heat transfer to concrete and gas evolution from the concrete.

7. SUMMARY AND CONCLUSIONS

7.1 Summary

An experimental investigation is reported whose objective is to provide an understanding of the thermal interaction between superheated core debris and water during postulated light-water reactor degraded core accidents. The experiment was designed to study the heat transfer characteristics of superheated spheres as they are either quenched by passage through a pool of water or as they are quenched in a packed bed configuration by an overlying pool of water. The work reported here was directed to the latter, i.e., to study the packed bed quenching process.

Stainless steel spheres, 3 mm in diameter, were heated in an oven to temperatures between 533 K and 977 K, and subsequently transferred to a vertical 108.2 mm i.d. stainless steel vessel. Water at temperatures between 274 K and 360 K was released on to the spheres and the resulting thermal interaction was observed. Packed beds of 40% porosity were studied, whose nominal heights were in the range 200 mm to 400 mm. The experiments were carried out at constant pressure, with the steam vented to the atmosphere. The wall of the test vessel could be preheated, if desired, to match the initial sphere temperature.

The test section was instrumented with an array of thermocouples, both within the pipe and on its outside wall. The interior thermocouples were positioned at the center of the pipe. A pressure transducer was mounted on the test vessel wall to monitor pressure fluctuations indicative of continued boiling within the vessel. All signals were recorded by a computer data acquisition system, were subsequently stored on magnetic tape, and eventually transferred to graphical paper output.

The thermocouple traces were used to infer the presence of either water or superheated spheres at the site of the thermocouples. The pressure transducer provided an estimate of the time that the water first contacted the bed, and the time period during which boiling continued within the test vessel.

Bed and wall temperature traces are presented for a range of experimental conditions. The bed thermocouples show a sequence of step changes in temperature, beginning with the uppermost one in the bed and proceeding downward. The temperatures suddenly drop from their initial values to the liquid saturation temperature. This sequential pattern of temperature reductions is interpreted to be indicative of a frontal cooling pattern which propagates down the column. It is a feature of nearly all of the data acquired in the experiments. It is believed that this initial sudden reduction in temperature is indicative of the first arrival of liquid to the site of the thermocouples. The wall temperatures generally show little temperature change during passage of the front. The position of the front as a function of time is obtained from analysis of the temperature traces and are presented as frontal propagation plots for each experimental run.

The temperature traces and frontal propagation plots indicate that the downward-moving front arrives at the base of the bed after a time delay which

depends on the bed depth and initial particle temperature. In many of the experiments the thermocouples indicate that a second front then moves up the column. The position of this front vs. time is extracted from the thermocouple data. The wall temperature also indicates passage of the upward-propagating front at times closely corresponding to the bed temperatures at the same axial locations, if the wall was initially heated to the bed temperature. The particle quench process is complete after passage of the upward-propagating front.

A direct measurement of the heat transfer rate between the bed and water was not made in these experiments. Several estimates of the heat transfer rate, however, are presented based upon the initial stored energy and various time scales which were extracted from the temperature traces and frontal propagation results. In addition, downward- and upward-frontal propagation speeds were computed from the data and are presented.

The heat transfer rate (per unit bed area) from the particle bed to water is estimated to have been in the range 1.0×10^6 to 2.5×10^6 W/m^2, independent of the initial particle temperature. The upper figure is an upper bound estimate of the heat transfer rate. The lower number of 10^6 W/m^2 represents an estimate of the average heat transfer rate over the duration of an experiment. This quantity is in reasonable agreement with predictions based upon the Lipinski (1980) steady-state debris bed heat transfer model, suggesting that two-phase countercurrent flow may also be a limiting factor in the transient heat removal from debris beds.

The data suggest that the superheated particle bed cooling rate, and hence the rate of steam generation, is limited by supply of liquid to the dry region of the bed. It is plausible that the supply of liquid, in the transient cooling experiments, is limited by a countercurrent two-phase flow mechanism. Additional data are required for further substantiation of this hypothesis.

7.2 Conclusions

The experiments reported here represent the first series in the program. The conclusions presented here are preliminary and will be evaluated further in future work.

The following major conclusions are drawn from the experimental work and their interpretation presented in this report:

- Superheated debris beds of uniform height which are cooled by an overlying pool of water transfer heat to the water in a two-stage frontal process. A cooling front first propagates down the bed. Upon reaching the bottom of the bed, a second front propagates upward.

- The lower region of the bed is dry and remains at the initial temperature until the first cooling front advances to that region.

- It is estimated that the average heat transfer rate (per unit bed area) over the quench time period was 10^6 W/m^2 for the

3-mm spheres used in the experiments. This heat transfer rate was independent of initial bed temperature and bed height.

- The magnitude of the average particle bed cooling rate in the transient quench experiments is consistent with the Lipinski (1980) steady-state debris bed heat removal model.

- The data suggest that the bed cooling rate is limited by the supply of liquid to the dry region of the bed. A plausible hypothesis is that the flow of liquid is limited by a two-phase counterflow mechanism, similar to that which limits decay heat removal from beds under steady state conditions.

- The MARCH HOTDROP single-particle heat transfer model assumptions lead to a conservative prediction of the estimated bed heat transfer rate (by one order-of-magnitude).

- A debris bed which settles in the reactor cavity with appreciable stored energy will immediately thermally attack the concrete basemat. The gases which are released from the concrete may further limit particle bed cooling.

ACKNOWLEDGEMENTS

The authors wish to express their gratitude to Dr. Ji-Wu Yang for many interesting and informative discussions on debris bed heat transfer behavior. We would like to thank Dr. Trevor Pratt for many helpful talks concerning the LWR licensing issues to which the work in this report is directed.

We are grateful to Dr. Narinder Tutu for providing a sounding board for ideas concerning interpretation of the experimental results and for his critical insights concerning the basic physical mechanisms. We acknowledge with thanks the work of Ms. Yako Sanborn who wrote the data acquisition and data reduction software used in the experiments, and who maintains the data acquisition system. On several occasions she came, cape in hand, to rescue data which were thought to be sunk to the depths of the data acquisition system. Thanks are also due to Dr. George A. Greene for his ideas on instrumentation concepts and their interpretation.

We wish to express our thanks to Mrs. Dorothy Thompson for her professional job of preparing this manuscript for publication.

REFERENCES

1. Barleon, L. and H. Werle, "Dependence of Debris Bed Dryout Heat Flux on Particle Diameter," Trans. Am. Nucl. Soc., 38, 382-3 (June 1981).

2. Bromley, L. A., "Heat Transfer in Stable Film Boiling," Chem. Eng. Prog., 46, 221 (1950).

3. Corradini, M. et al., "Light Water Reactor Safety Research Program Quarterly Report, April-June 1980," Sandia National Laboratory, NUREG/CR-1509 (August 1980).

4. Denton, H. P., NRC Memorandum (March 17, 1980).

5. Dhir, Y. K. and I. Catton, "Study of Dryout Heat Fluxes in Beds of Inductively Heated Particles," NUREG-0262, U. S. Nuclear Regulatory Commission (1977).

6. Dhir, Y. K. and I. Catton, "Dryout Heat Fluxes in Debris Beds Cooled at the Bottom and Having Subcooled Liquid at the Top," Nucl. Tech., 46, 356 (1979).

7. Gabor, J. D. et al., "Status Report on Limiting Heat Fluxes in Debris Beds," Argonne National Laboratory, ANL/RAS 80-21 (September 1981).

8. Ginsberg, T., "Safety Research Programs Sponsored by Office of Nuclear Regulatory Research, Quarterly Progress Report, July 1 - September 30, 1981," BNL-NUREG-51454, Vol. 1 (November 1981).

9. Gronager, J. E. et al., "Advanced Reactor Safety Research, Quarterly Report, January-March 1980," Sandia National Laboratories, SAND 80-1646 (April 1981).

10. Hardee, H. C. and R. N. Nelson, "Natural Convection in Porous Media with Heat Generation," Nuc. Sci. & Eng., 63, 119-32 (1977).

11. Lipinski, R. J., "A Particle-Bed Dryout Model with Upward and Downward Boiling," Trans. Amer. Nucl. Soc., 35, 358 (1980).

12. Meyer, J. F., "Preliminary Assessment of Core Melt Accidents at the Zion and Indian Point Nuclear Power Plants and Strategies for Mitigating Their Effects," Vol. 1, Nuclear Regulatory Commission Report, NUREG-0850 (November 1981).

13. Ostenson, R. W. and R. J. Lipinski, "A Particle Bed Dryout Model Based on Flooding," Nuc. Sci. & Eng., 79, 110-113 (1981).

14. Pratt, W. T. and R. A. Bari, "Containment Response During Degraded Core Accidents Initiated by Transients and Small Break LOCA in the Zion/Indian Point Reactor Plants," Brookhaven National Laboratory, BNL-NUREG-51415 (July 1981).

REFERENCES
(Cont'd)

15. Rasmussen, N. C., "Reactor Safety Study," U. S. Nuclear Regulatory Commission, WASH-1400 (October 1975).

16. Shires, G. L. and G. F. Stevens, "Dryout During Boiling in Heated Particulate Beds," AEEW-M1779, U.K. Atomic Energy Authority, Winfrith (1980).

17. Theofanus, T. G. and M. Saito, "An Assessment of Class 9 (Core Melt) Accidents for PWR Dry Containment Systems," Purdue University, PNE-81-148 (June 1981).

18. Wooton, R. O. and H. I. Avci, "MARCH (Meltdown Accident Response Characteristics) Code Description and User's Manual," Battelle Columbus Laboratories, NUREG/CR-1711 (October 1980).

19. Yang, J. W., "Cooling of Core Debris and the Impact on Containment Pressure," Brookhaven National Laboratory, NUREG/CR-2066 (July 1981).

20. Zuber, N., "Hydrodynamic Aspects of Boiling," Dissertation, Univ. of California, AECU-4439 (1959).